Coherent noise attenuation in the radial trace domain: introduction and demonstration

David C. Henley

ABSTRACT

The radial trace transform is a simple mapping of seismic data from the familiar horizontal distance and travel time (X-T) domain of trace gathers and stacked sections to the domain of apparent velocity and travel time. The transform has properties that make it well-suited for such practical applications in seismic processing as wavefield separation and coherent noise attenuation. We describe here the transform and its practical implementation, including aliasing considerations, and we demonstrate linear noise attenuation on both model data and field data using a set of ProMAX modules which we have developed to apply R-T domain techniques.

Radial trace (R-T) domain filtering techniques are distinguished by their focus on localized events in the X-T plane rather than widespread families of events with common frequency and/or wavenumber characteristics as in F-K (frequency and wavenumber) domain methods. A number of successive radial trace filter passes can be applied to X-T trace panels, each pass designed to attenuate one or more specific events. Furthermore, the radial trace transform can be applied to panels with highly irregular X intervals, unlike the F-K transform. This makes the radial domain very attractive for filtering coherent noise on 3-D shot gathers, with their non-linear distributions of source-receiver offsets, since the data need not be interpolated to a uniform offset grid prior to filtering, as with F-K filtering.

INTRODUCTION

Geophysicists who are familiar with the radial trace transform usually associate it with attenuation of multiples (Taner, 1980), (Lamont, et al, 1999), or with migration and imaging algorithms (Ottolini, 1979). It appeared in the early reports from the Stanford Exploration Project, but is only sparsely represented in public geophysics literature compared to integral transforms such as the F-K or τ-p transforms. As with all 2-D transforms, the motivation for the use of the radial trace transform lies in its useful rearrangement of geometrical relationships represented in the familiar X-T plane in which most seismic data are recorded and displayed. Specifically, the radial trace transform maps a wavefield into the domain of apparent velocity and travel time, or, nearly equivalently, takeoff angle and travel time. This mapping makes the radial trace domain attractive for multiple suppression. In a constant-velocity, horizontally bounded medium, the raypath of a primary reflection on a constant-takeoff angle trace coincides with the raypath of the first leg of any simple multiple on the same trace (Taner, 1980). This ensures that the travel time of the multiple on a radial trace is an integral multiple of the primary travel time. Also, the angle-dependent reflectivity of the multiple-producing boundary is the same for the primary reflection and at least the first bounce of the multiple. The basic assumptions for most prediction-based multiple rejection algorithms are therefore more nearly satisfied in the radial trace domain than in the conventional X-T domain.

A feature of the radial trace transform which appears to have been largely neglected except for an early SEP report (Claerbout, 1983), is the fact that linear events in the original X-T domain whose apparent velocity and origin nearly match those of one or more radial traces into which they map have their apparent frequencies dramatically lowered. An unaliased linear event in X-T whose apparent origin coincides with that of the radial trace (R-T) transform maps to a small set of DC or near-DC traces in the radial domain. Locating the origin of a radial trace transform at or near the source position of a source gather, therefore, transfers widespread source-generated noise to a few radial traces of very low frequency while leaving the hyperbolic reflected events nearly unaffected. Coherent noise rejection can hence be accomplished by low-cut filtering and/or trace scaling in the radial trace domain, and the filtered X-T panel can be recovered via the inverse radial transform.

This same radial transform feature can be used to affect wavefield separation of a desired linear mode simply by placing the origin of the transform at the apparent origin of the mode. In this case, the application of a low-pass filter in the radial trace (R-T) domain preserves the desired linear mode while attenuating high-frequency reflections and similar events, (a process anticipated by Claerbout, pp 45-47 in his demonstration of the removal of aliasing from ground roll).

Design of R-T filters for linear noise attenuation or linear wavefield separation is direct and intuitive and is always aimed at specific events, unlike F-K filters, which attenuate or enhance all events with similar frequency-wavenumber characteristics. Consequently, an R-T filter may be designed to attenuate a linear event at a particular apparent velocity while leaving the long-offset limb of a reflected event with the same apparent velocity unaffected.

METHOD

The radial trace transform

The elementary radial trace transform R is a simple mapping of the amplitudes of seismic traces S whose co-ordinates are source-receiver offset x (or some other lateral distance from a single reference point) and two-way travel time t to the new co-ordinates apparent velocity v and two-way travel time t'. The transform is defined by:

$$R\{S(x,t)\} = S'(v,t'), \tag{1}$$

with the inverse given by:

$$R^{-1}\{S'(v,t')\} = S(x,t), \tag{2}$$

where

$$t' = t; \;\; v = x/t. \tag{3}$$

A nearly equivalent mapping in terms of two-way travel time and takeoff angle can be described by:

$$t' = t; \quad \theta = \arctan(x/t). \tag{4}$$

Practically, these two descriptions differ only in the increment of the angular co-ordinate, which differs significantly only for large v (or θ) . The parameterization in terms of velocity is generally more computationally convenient.

Figure 1 is a schematic illustration of the process of mapping a seismic shot gather from the conventional X-T domain to the radial trace (R-T) domain. As can be seen from the figure, each radial trace consists of samples gathered along a linear trajectory of constant apparent velocity (or angle), *using the same sample times* as the original X-T trace samples. The fact that X-T and R-T domains share the same time scale is important. This determines the relative *duration* of an event in the two domains, where we define duration as the number of samples occupied by an event waveform on a single trace in either the X-T or R-T domain. Event *duration* is the same in both domains *only for events parallel to timing lines*. An event parallel to timing lines transforms from X-T to R-T with its frequency content unchanged. However, an event *not* parallel to timing lines has a different *duration* in the R-T domain than in the X-T domain, being either stretched or compressed, depending upon the angle the event wavefront makes with R-T trace trajectories. For an event whose wavefront is nearly parallel to an R-T trajectory, its duration is greatly increased in the R-T domain, since the R-T amplitudes will be selected from nearly the same point of the event waveform on every X-T trace. This effectively stretches the event duration, thus lowering its apparent frequency. Conversely, an event whose wavefront is nearly *perpendicular* to an R-T trajectory will have its duration *decreased* relative to the X-T traces, and hence its apparent frequency increased in the R-T domain.

It is evident from figure 1 that many radial trace samples will fall between the original X-T traces, requiring interpolation of values from the nearest X-T traces. In the R-T transform, various interpolation schemes can be chosen, depending upon the particular R-T application selected. For the forward and inverse R-T transforms which we have developed, we have chosen to interpolate parallel to lines of constant travel time using simple and fast two-point algorithms. Interpolation is discussed more thoroughly in a companion chapter (Henley, 1999,1) in this volume.

Figure 2 follows from figure 1 and shows representative radial traces corresponding to the numbered trajectories across the X-T panel in figure 1. We display only a few of the R-T traces that would be generated using the set of R-T trajectories in figure 1 so that we may more easily see details. In figure 2 we illustrate the event stretching, or change of apparent frequency, due to the R-T transform, on a linear event whose origin and slope make it nearly parallel to some of the R-T trajectories that span it. Since those trajectories encounter the event at nearly the same point on its waveform on every X-T trace, the amplitudes they map into the R-T domain will vary only very slowly with travel time, hence increasing the apparent duration of the event and lowering its apparent frequency. This is illustrated by radial traces 1 and 2 in figure 2, which cross the linear event at very small angles. Traces 3, 4 and 5 encounter the linear event at much larger angles and show correspondingly less stretching for the linear event. None of the R-T trajectories in figure 1 cross the reflections at small angles, so the reflection duration, and thus their frequency content is relatively unchanged by the R-T transform.

In general, the radial traces corresponding to higher velocities encounter the far offset X-T trace well before the end of the range of X-T travel times, so the high velocity R-T traces have fewer live samples than their lower velocity counterparts. This explains the shape of the typical R-T transform, with shorter traces at higher velocities.

Figure 1 also illustrates the fact that while the R-T transform maps any X-T domain value to the R-T domain, it does so in a non-uniform fashion; amplitudes at small offsets and small travel times tend to be over-sampled and those at greater times and offsets under-sampled, due to the divergence of the radial trace trajectories. For this reason, we normally specify more traces in the R-T domain than in the original X-T domain, an attempt to minimize aliasing in the transform and ensure its invertibility. Referring to figure 1, we can see that the greatest risk of aliasing of the X-T panel by the R-T trajectories occurs where the R-T trajectories are spread the widest, at the outer edges of the X-T panel. If we choose a radial trace density great enough that the R-T trajectories are no more than one sample apart on the outer edges of the X-T panel, we ensure that every sample in the X-T domain contributes to *at least* one sample in the R-T domain. This prevents aliasing of X-T amplitudes in the R-T domain *by the mapping process* and enables the full recovery of the X-T panel by the inverse R-T transform, which can be envisioned as the extraction of amplitudes at each sample time from the nearest R-T traces along constant-X trajectories in the R-T domain.

An interesting feature of the R-T transform and its inverse is that one need not transform the entire X-T panel. The inverse R-T transform can easily fit R-T samples back into the original X-T panel after some operation in the R-T domain while leaving the non-transformed X-T data untouched. Furthermore, the formula (3) can be generalized to allow placement of the radial trace origin at any arbitrary point (x_0, t_0) in the X-T plane;

$$t' = t - t_0;\ v = (x - x_0)/(t - t_0). \tag{5}$$

The utility of this feature will be seen in more detail in the examples shown.

Operations in the R-T domain

We can apply a number of seismic processing algorithms to R-T traces to accomplish useful objectives, as long as we do nothing that increases inherent aliasing in the R-T domain (to facilitate inversion back to X-T). As an example, multiple attenuation (Taner, 1980), (Lamont, et al., 1999) is accomplished by predictive filtering of the R-T traces, but we need to take care in using any operation that whitens the spectrum in the R-T domain, since this increases the risk of introducing spatial aliasing back in the X-T domain. We will not treat deconvolution techniques here, but will focus on linear event attenuation and enhancement techniques, which generally *reduce* the spectral bandwidth rather than increase it.

Two features of the R-T transforms of seismic gathers can be utilized to accomplish either wavefield separation or linear noise attenuation; the previously described event stretching, and the discretization of linear events spread across many traces in an X-T gather into much smaller sets of R-T traces within the transform. The latter feature

means that linear event amplitude can be changed simply by rescaling the R-T traces containing the event relative to the neighboring R-T traces. Processing algorithms which can be used in the R-T domain to attenuate or enhance linear events include:

- time or frequency domain low-pass, high-pass, band-pass filtering,
- frequency domain spectral editing (spike clipping, notch filling),
- trace-to-trace amplitude equalization,
- AGC.

Terminology

In what follows, our terminology will be as follows:

- R-T transform means the mapping of seismic amplitudes from the X-T domain to the radial trace (R-T) domain.
- Inverse R-T transform means the mapping of seismic amplitudes from the radial trace (R-T) domain to the X-T domain.
- R-T filter means an R-T transform, followed by a time or frequency filter pass and/or R-T trace amplitude scaling, followed by an inverse R-T transform.
- R-T fan filter means using an R-T transform and inverse having a wide range of apparent velocities and an origin in the near vicinity of the seismic source for the X-T trace panel. The objective is to effectively transform overtly source-generated events for attenuation or enhancement.
- R-T dip filter means using an R-T transform and inverse having a narrow range of apparent velocities and an origin distant from the X-T panel. The motivation here is to transform parallel dipping events for effective attenuation or separation.

Fan filtering

To attenuate source-generated linear noise events on source (or receiver) gathers, which typically cover a range of velocities including the very slow air blast as well as relatively fast refracted and direct waves, the X-T gather must be examined to determine the position of the apparent origin of the events (or at least the strongest ones). From this origin, the apparent velocity limits of a fan covering all the offending noises can be determined. In most cases, for source-generated noise, these velocity limits should include the entire gather, since the direct arrival is linear noise that we may wish to eliminate. Using the origin and velocity limits determined from the gather, the X-T traces are transformed to the R-T domain. Linear noise may be attenuated by low-cut filtering of the R-T traces, using filter parameters comparable to low-cut parameters that might be used in the corresponding X-T domain. If particular linear events are especially strong, then following the filtering with trace equalization or AGC can result in additional attenuation. It should be recognized,

however, that once relative trace amplitudes are altered in the R-T domain they cannot be restored in the X-T domain.

If the linear noise on a gather seems to emanate from more than one origin (surface wave plus a deep refraction, for example), an R-T fan filter pass can be applied at each apparent origin. Repeated R-T filter passes seem to cause little degradation of the unattenuated modes, except that repeated application of a given filter has the effect of steepening the roll-off slopes of the effective filter band (the amplitude spectrum of the filter is multiplied by itself for each additional filter pass). For a high-pass R-T filter this has little consequence; but for a band-pass R-T filter, the higher frequencies associated with reflections we desire to preserve may be adversely affected. Static shifts and other lateral discontinuities in the original X-T panel, such as geological faults, 60 Hz traces and amplitude-reversed traces, will survive more than one pass of radial trace filtering without lateral smearing, given appropriate R-T transform design.

A useful technique for filtering a wide variety of shot records is to apply an ordinary radial fan filter with origin at or near the shot origin, then to apply a fan filter with origin located at a 'virtual source' point for the 'back-scattered' linear noise that often becomes apparent after the first radial filter pass. Since this noise typically dips inward towards the zero offset trace, it appears to have an approximate virtual source at a point *below* the gather at zero offset. In practice, we accomplish this inverted radial fan filter application by time-reversing the X-T traces prior to the R-T filter pass and time-reversing them again after the pass. The R-T transform origin is then chosen at some point *above* the time-reversed gather.

The special case of dispersive linear noises can be effectively addressed in the R-T domain due to the particular geometry of the R-T transform. If a noise is noticeably dispersed (different frequency components travelling at different velocities), as with some examples of ground-roll, or the notoriously powerful ice-wave observed in the arctic, then individual radial traces will tend to isolate specific frequency components of the linear noise. We can then compute the 1-D Fourier transform of each R-T trace to move to the radial frequency (R-F) domain. In this domain, superimposed upon the seismic signal spectrum on each R-F trace will be a large amplitude spike at the frequency of the particular component of the dispersed noise captured by the original R-T trace. An effective technique for attenuating the noise consists of replacing the spectral amplitude values in the vicinity of the spike with corresponding values from the running median of the spectrum (spectral clipping) on each R-F trace. The noise-free R-T traces can then be recovered from the R-F domain via the inverse 1-D Fourier transform, and the R-T traces transformed back to X-T via the usual inverse R-T transform. Being non-linear, this method can attenuate some examples of dispersed noise more effectively than strictly linear methods. While we don't demonstrate this technique here, it has been shown in early radial trace filtering examples at Shell Canada and will be implemented in a later version of CREWES software.

If a processing objective is to enhance linear events on a panel of seismic traces, this can be accomplished quite effectively by a low-pass filter in the R-T domain. Alternatively, linear noise attenuation can be accomplished by subtraction of these

low-pass R-T filtered data from the original X-T panel. In this case, care must be taken *not* to alter the relative amplitudes of the traces in the R-T domain with trace equalization or AGC. In general, the subtraction method does not seem to be as effective as the more straightforward low-cut filter in the R-T domain, although it may work better in cases where the linear noise is badly aliased and thus less susceptible to low-cut R-T filtering.

Dip filtering

Since we can locate the origin of a radial trace transform at any point within the 2-D space containing the panel of traces to be filtered, we can emulate a dip filter by placing the origin of a narrow fan of radial traces at a great distance from the actual panel of seismic traces. Since the range of apparent velocities of the radial traces will be small (the distance to the 'virtual origin' determines the velocity range), we effectively span the input trace panel with 'dip trace' trajectories of nearly constant velocity. In this case, any linear noise aligned with radial traces will have very low apparent frequencies in the R-T dip domain and can be attenuated with a low-cut filter. This mode of operation thus emulates one kind of F-K filtering, but like all radial operations, has the advantage of preserving lateral discontinuities like statics.

Because we often encounter linear noise of relatively constant dip on stacked sections, the radial dip filter operation is attractive for noise removal in such sections. Simply by appending some phony source-receiver offset trace headers, sections can be dip filtered as if they were shot or receiver gathers. Dip filtering is better illustrated in another chapter of this report (Henley, 1999, 2)

Software

We have developed a set of ProMAX modules to apply R-T domain processing to seismic trace panels. These include a module to apply both R-T fan filters and dip filters to a trace panel, a module to perform the R-T transform and its inverse for both the fan and dip configurations, and a module to perform the forward R-T transform only, for R-T domain display purposes. The software is described more completely in another chapter of this report (Henley, 1999, 1).

EXAMPLES

Application to field data: Blackfoot

To illustrate and illuminate the use of R-T domain filtering techniques, we use one of the 2-D 3-C data sets acquired at the PanCanadian Blackfoot field during the course of extensive seismic work conducted over several years at that location in order to help delineate the target channels that comprise the hydrocarbon reservoir (Simin et al., 1996), (Miller et al., 1995). We have chosen the records corresponding to the vertical component of a 2-D 3-C seismic line over the Blackfoot field. There are 151 stations on the line, spaced 20 metres apart; and all stations were shot for this experiment, making receiver gathers usable for filtering as well. Figure 3 shows two typical shot gathers from this line. While linear noise is evident on these gathers, the level is not excessive, and these data can be successfully imaged without an explicit

noise attenuation procedure. We use these data, therefore, only to demonstrate the application of the radial trace technique, not to lobby for its preferential use. On these records we can see two main types of linear noise; direct arrivals and shallow refractions near the top of the records, and ground-roll and air-blast dominating the central portion of the records. The direct arrivals and refractions obscure shallow reflections at larger offsets while the air-blast and ground roll dominate the deeper reflections at smaller offsets. Spatial aliasing is prominent for the air-blast and ground roll.

The same two records are shown in figure 4 after a single pass of an R-T domain fan filter with the low-cut at 15 Hz. In comparison with figure 3, improved amplitude and lateral continuity for all reflections is evident, particularly those previously obscured by the shallow refractions. Some apparent "back-scattered" noise inclined towards the centre of each gather has become more visible as a result of the radial filter pass. An additional radial fan filter pass, this time with the traces time reversed to give the effect of a radial filter positioned at a virtual source below the gather, results in the panels in figure 5. There is dramatic improvement of reflection continuity at all levels, and, compared with figure 3, visible static shifts have been preserved from the original record. This means that the filtered trace gathers can still be used for residual statics estimation, possibly more successfully than the raw gathers, due to the reduction of interfering noise.

Low-pass R-T filtered shot gathers appear in figure 6. This is approximately the same as the noise filtered out by one high-pass R-T fan filter. The result of subtracting this noise from the original panels is shown in figure 7. The results are evidently not as good on this example as those obtained with a straightforward application of a low-cut filter in the R-T domain (figure 4). Experimentation with filter parameters might lead to better results in this case.

Figure 8 shows the raw shot gathers in the R-T domain. It can easily be seen that the direct arrivals and refractions have been rotated to near vertical orientations, such that their apparent frequency is very low. The ground-roll and air-blast have not undergone such great changes, but their frequencies have been lowered nevertheless, increasing their susceptibility to low-cut filtering. Reflections on these records have been changed little in appearance from those on the X-T gathers of figure 3. The result of application of a low-cut filter to these R-T traces can be seen in figure 9. Trace amplitudes have not been re-normalized following the filter application, so that the figures convey an impression of energy removal from various portions of the R-T panels.

Noise reduction on shot gathers makes little sense if no improvement is realized on a stacked section. Therefore, we use CDP stacks to compare shot gathers which have been R-T filtered with those which have not. For these comparisons, we apply a simple NMO correction and neglect statics corrections, since statics in the Blackfoot area are small for compressional waves. As statics derivation can vary significantly for data traces with different levels and kinds of noise, R-T filtering should *improve* statics derivation, however. We are demonstrating here *only* the explicit improvement of image due to linear noise reduction techniques.

As our control image for comparison, figure 10 shows a CDP stack of shot gathers whose X-T traces have been low-cut filtered at 15 Hz and NMO corrected. No initial muting or statics have been applied. It can be seen that the 15 Hz low-cut and the stacking process have removed much of the coherent noise, as anticipated. Figure 11 contains a comparable stack of shot gathers which have received one application of R-T domain fan filtering, with the same low-cut at 15 Hz. Differences between the two sections are relatively small, but the shallow portion of the section has been significantly improved by the R-T domain filter, which has removed the direct arrival, thus improving the shallow part of the stack. Small improvements can also be seen near the edges of the section, where the stack fold decreases. In other words, when noise attenuation due to stacking is less effective, the attenuation due to R-T filtering is more apparent. We followed the initial R-T fan filter on shot gathers with another R-T fan filter on inverted shots (for 'back-scatter'), then applied an R-T fan filter to receiver gathers. The stack of these data is featured in figure 12. The improvement in this section is significant compared to the brute section in figure 10. Noise amplitudes have decreased and event continuity has improved over most of the section, even near the low-fold edges. Some residual coherent noise is still visible on this section, however, and we can apply R-T domain dip filters to the section to remove most of this, as shown in figure 13. As a final cosmetic step for this comparison, we applied a mild predictive deconvolution to the stack traces, followed by F-X deconvolution (figure 14). The brute stack, after application of the same post-stack deconvolution operations, appears in figure 15. At this point, it becomes evident that the coherent noise attenuation affected by the R-T filtering has made significant changes in the appearance of the imaged data. In spite of repeated filter passes, the section in figure 14 shows more apparent recovered signal bandwidth than the brute stack of traces filtered only once with a 15 Hz low-cut in the X-T domain.

To examine the stack differences in more detail, we compare close-up views of a small zone centered on one of the target channels in the next few figures. Figure 16 shows this channel zone as it appears on the brute stack section, while the pre- and post-stack R-T filtered version is displayed in figure 17. The differences are remarkably small on this portion of the section, where stack-fold is high. However, when we compare the post-stack deconvolutions of these stacks in figures 18 and 19, respectively, we see major differences in the appearance of the data. The character of the channel anomaly is significantly different on the two versions of the stack, and the differences are probably attributable to the R-T domain coherent noise removal. A section actually used for interpretation would undergo significantly more sophisticated processing than either of these examples, however, likely including pre-stack deconvolution, residual statics, and some type of migration.

Model study

In order to better understand some of the merits of R-T domain filtering with respect to the more widely used F-K domain filtering, we constructed a synthetic model shot gather and placed some pseudo-random statics in the trace headers to be applied to the traces prior to filtering in order to compare lateral smearing for the different techniques. Smearing by F-K methods is attributable to the spatial convolution of the truncated X-T impulse response of the F-K domain filter with the traces of an input X-T panel. Smearing by R-T methods is attributable to two effects: convolution of the

filter impulse response, similar to the X-T application of F-K filters, and the intrinsic X-direction interpolation used by the R-T transform and its inverse to move from the X-T to the R-T domain and vice versa. In the R-T transform, we always choose finite velocities for the radial traces, so the filter impulse response in the X-T domain, which extends only along R-T trace trajectories, will never have a component explicitly aligned with the X-direction and will never intrinsically smear horizontally. The X-direction *interpolation* method in the transform, however, can lead to significant lateral smearing if not carefully chosen. We test here a simple interpolation method that minimizes this smearing.

The synthetic shot gather created for the test (figure 20) contains five reflection-like events with hyperbolic moveout and two linear events, one fast and unaliased, the other slower and close to the spatial alias threshold. Event amplitudes are such that the two linear events are stronger than the underlying reflections, as is typical for real shot gathers. When doing visual comparisons on these synthetic data, we identify the signal/noise ratio approximately with the ratio of the peak amplitude of the desired event to the peak amplitude of the undesired one. Figure 21 shows the synthetic gather after application of a typical R-T domain fan filter. The fast linear event has been almost totally removed, while the slower event has been significantly attenuated, but survives due partly to the fact that the first R-T filter origin does not coincide with the event origin. We apply a second R-T filter at this event origin, the result of which is shown in figure 22. The slow linear event has been much reduced in amplitude, but some energy at spatially aliased frequencies remains. We next examine the result of applying an F-K velocity filter in the reject mode (cut events with velocity *lower* than that of reflections) to the synthetic model (figure 23). The traces on the gather have *not* been re-normalized after filtering. The low velocity linear event has been relatively well attenuated, but the high velocity event still retains much of its energy. The result of applying an F-K velocity filter in the boost mode (boost events having *higher* velocity than noise) to the synthetic shot gather appears in figure 24. Again, traces have not been re-normalized after filter application. In this case, the low velocity linear event has been almost totally removed, and the high velocity one significantly attenuated.

We examine these results in more detail in figure 25, which shows a close-up of the portion of the synthetic gather where the slow linear event crosses the reflection events. The same close-up after one pass of the R-T fan filter, and two R-T filter passes (the second at the slow event origin) are shown in figures 26 and 27, respectively. Figures 28 and 29 are the results of the F-K velocity reject and velocity boost filter passes. From these results, it appears that the F-K boost filter is the most effective for attenuating the slow linear event, while the R-T fan filter is the most effective against the fast linear event, and the two-pass R-T combination is the most effective overall. Little attempt was made in this study to design the *best* coherent noise filter either in the R-T domain or in the F-K domain; this study is meant only as a quick illustration of some of the differences in the two techniques. We chose to test the velocity wedge F-K filters because of the similarity of some of their key design parameters to those in R-T filters, specifically velocity limits.

We next explore the effect of applying each of the filters described above to data having uncorrected statics, since prior to filtering, we are often unable to reliably

derive and remove statics on very noisy shot gathers. Figure 30 shows the synthetic shot gather with pseudo-random statics applied to the traces. The statics affect the linear events as well as the reflections and will degrade filter performance by mis-aligning the noise events. The synthetic shot with statics after one pass of R-T fan filtering is shown next in figure 31. As anticipated, filter performance has been compromised somewhat, particularly on the fast linear event, but the static shifts on the trace events remain apparently unaffected by the filter process. The result for two R-T fan filter passes in figure 32 shows that the second R-T pass has further reduced linear event amplitude while affecting statics very little, except for the appearance of some small side-lobes on the reflection events due to filter response tails from the R-T domain. These are visible only on synthetics with widely spaced events separated by explicitly zeroed dead zones. Figure 33 is the result of applying the F-K velocity reject filter to the synthetic with statics. We note somewhat less effective filtering than in the no-statics case in figure 23, but we see that the original statics have been well-preserved, with almost no side-lobes. Figure 34 demonstrates the comparable result for the F-K velocity boost filter. Once again, we see some decrease in filter effectiveness, though the low velocity linear event is still strongly attenuated. This filter, however, destroys virtually all statics information; we see the classical smearing effect often attributed to F-K filters.

To see more detail, we look once again at close-ups of the above records. Figure 35 is the same close-up view as figure 25, but with the trace header statics applied. The close-up appears again in figure 36 after one R-T fan filter pass, while figure 37 demonstrates the effects of two R-T filter passes. While filter response tails have created some side-lobe energy in the dead zones of the synthetic gather, the reflection events remain quite clear and easily correlated, with no apparent affect on their static shifts. The close-up after F-K velocity reject filtering is shown in figure 38. The static shifts are preserved in this case, as well, but reflection amplitudes show variations that could degrade the performance of an automatic correlation algorithm. In figure 39, we confirm that F-K velocity boost filtering, while effectively removing the low velocity linear event, also destroys all statics information.

In figure 40, we show a close-up of a different part of the synthetic gather, at larger offsets than the previous close-up. In this portion of the synthetic, radial traces in the R-T transform span the gather at smaller angles to the horizontal, and might therefore be expected to have more of a lateral smearing effect on statics. Indeed, in figure 41 where one pass of R-T fan filtering has been applied, we can find several examples where reflection amplitude and/or character have apparently suffered from the radial filter application, typically where the local slope of a trace-to-trace static shift is the same as the slope of the radial trace in the R-T transform. This alignment leads to smearing of the event along the radial trace direction by the filter response function. Fortuitously, however, this alignment of local static shift slope with radial trace slope can occur only once per trace *for a given static shift*; so that if one event on an X-T trace is affected, the other events will be less so, and the static is consistently correlatable on the other events on the trace. Figure 42 illustrates the effect of applying two passes of R-T fan filtering to the gather. The preservation of statics by the velocity reject mode of F-K filtering is well-illustrated in figure 43, and their total smearing by the velocity boost F-K filter is shown in figure 44.

What this limited study has shown is that R-T domain filtering can be very effective while still preserving lateral trace-to-trace variations such as statics. More effective filtering of low velocity linear events can be done in the F-K boost mode, but only with accompanying smear of lateral details. These can be preserved using the F-K reject mode, but noise attenuation is not as effective then.

DISCUSSION

Results

We have demonstrated a new technique for wavefield separation and coherent noise attenuation based on the radial trace transform. Further, we have shown that it can be effective in attenuating noise while preserving lateral detail in panels of traces to which it is applied. Because it is a simple mapping, the radial trace transform is easy to compute and invertible, if precautions are taken to avoid aliasing. Transform design parameters are easily related intuitively to coherent events on panels of seismic traces; and in some filter applications, it can be more effective than the more traditional F-K transform. Unlike F-K filters, R-T domain filters can be applied repeatedly, so that several passes can be applied to a single gather or panel, each pass directed at a particular type or mode of coherent noise (Henley, 1999, cas1). Also unlike F-K filtering, R-T domain operations do not require that the original data panel be uniformly gridded in either X or T, since any point in the R-T domain can be appropriately determined by interpolation from existing points in the X-T domain. Also, the entire X-T domain does not need to be mapped into the R-T domain. Any subset can be completely transformed from the X-T plane to the R-T domain and back. The latter two properties of the R-T transform can provide a real advantage over an integral transform like the F-K for some applications.

Situations where R-T domain filtering should be considered as an alternative to F-K filtering are as follows:

- source or receiver gathers with very strong coherent noise emanating from one or more apparent source points on or near the gather, where an imagined overlay of radial trace trajectories on the gather would show considerable alignment between radial traces and coherent noise wavefronts.

- source or receiver gathers with strong first arrival noise masking shallow reflections at larger offsets.

- source or receiver gathers with irregular distributions of source-receiver offsets

- gathers with linear noise demonstrating large dispersion (ground-roll, ice-wave)

- lines with low stack-fold and high levels of coherent noise

- stacked sections exhibiting residual dipping coherent noise from incomplete pre-stack filtering (R-T dip filter)

- gathers with such low signal/noise ratios that reflections are badly obscured, on which it is not possible to find and remove statics prior to coherent noise removal

- gathers on which reflections and coherent noise have the same dip, but different origins

Extensions and further development

To this point, we have discussed only one broad application for the radial trace transform, that comprised of wavefield separation and coherent noise attenuation. Only the simplest form of the transform has been presented for this application. There are many interesting modifications that can be made to the basic transform that can materially expand its usefulness for geophysical applications. One of the simplest is the incorporation of a means for curving the radial trace trajectories of the transform. This allows the radial traces to better fit some types of coherent events and thus to affect a better separation of these events in the R-T domain. A variation of this idea would allow radial traces to follow the trajectories of raypaths projected into the subsurface through a velocity model (Ottolini, 1988). Transforming gathers using such a raytracing scheme and sorting the resulting R-T traces into common-apparent-velocity panels would yield panels on which Amplitude-vs-Angle (AVA) effects should be apparent (Claerbout, 1983), which may be useful for analysis of angle-dependent phenomena. We intend to pursue this potential application.

Because of the irregularity of offset distributions in 3-D shot gathers, rejecting coherent noise is difficult using F-K techniques. The R-T filter technique can be applied without modification, by treating each receiver-line spread like a 2-D shot gather and using the source-receiver offsets from the trace headers. Because source-generated noise is most coherent and least aliased in the receiver line gathers, these are the appropriate gathers to which to apply the filter.

Since the R-T transform is an interpolating transform, it can be used to regularize input trace gathers by replacing the source-receiver offsets of the original X-T traces input to the forward transform with a new set of offsets in the inverse transform. Likewise, the trace amplitudes can be re-gridded to a new set of travel times in the inverse R-T transform. We have made provision in the current software for re-gridding an input gather to the X-T, the X**2-T, or the X**2-T**2 domains. The latter is particularly useful, since all hyperbolic events map to straight lines. In this domain, not only do hyperbolic events become linear, but reflections have nearly *the same* linear moveout while multiples or other wave modes like shear waves have a *different* linear moveout at the same travel times. This may afford an opportunity for effective wavefield separation for P and converted modes recorded on the same shot panels. Likely, both the R-T and τ-p domains would prove useful in this context. We intend to investigate the X**2-T**2 domain further for other potential applications.

Multiple attenuation in the R-T domain has been demonstrated by others, but we hope to investigate this application area as well.

ACKNOWLEDGEMENTS

The author gratefully acknowledges the support of CREWES and its sponsors in this work. Discussions with various staff members (Peter Cary, Pat Daley, Gary Margrave), as well as assistance with programming details (Peter Cary, Henry Bland) were an important part of this work. The permission of Shell Canada Ltd. and the Shell Group to release this work, begun at Shell Canada, for further research and development is also gratefully acknowledged. Thanks also to former colleagues at Shell for much discussion, many trial data sets, and a lot of support.

REFERENCES

Claerbout, J.F., 1983, Ground Roll and Radial Traces, Stanford Exploration Project Report, SEP-35, pp 43-53.

Henley, D.C., 1999, Radial trace computational algorithms at CREWES, CREWES Research Report **11**.

Henley, D.C., 1999, Demonstration of radial trace domain filtering on the Shaganappi 1998 geotechnical survey, CREWES Research Report **11**.

Lamont, M.G., Hartley, B.M., and Uren, N.F., 1999, Multiple attenuation using the MMO and ISR preconditioning transforms: The Leading Edge, 18, no. 1, 110-114.

Miller, S.L.M., Aydemer, E.O., and Margrave, G.F., 1995, Preliminary interpretation of P-P and P-S seismic data from the Blackfoot broad-band survey. CREWES Research Report **7**, Ch. 42.

Ottolini, R., 1979, Migration of Radial Trace Sections, Stanford Exploration Project Report, SEP-20, pp 97-115.

Ottolini, R., 1981, Downward Continuation of Common Midpoint Gathers by Transformation into Snell Trace Coordinates, Stanford Exploration Project Report, SEP-26, pp 83-94.

Simin, V., Harrison, M.P., and Lorentz, G.A., 1996. Processing the Blackfoot 3C-3D seismic survey. CREWES Research Report **8**, Ch. 39.

Taner, M.T., 1980, Long-period sea-floor multiples and their suppression: Geophys. Prosp., 28, no. 1, 30-48.

FIGURES

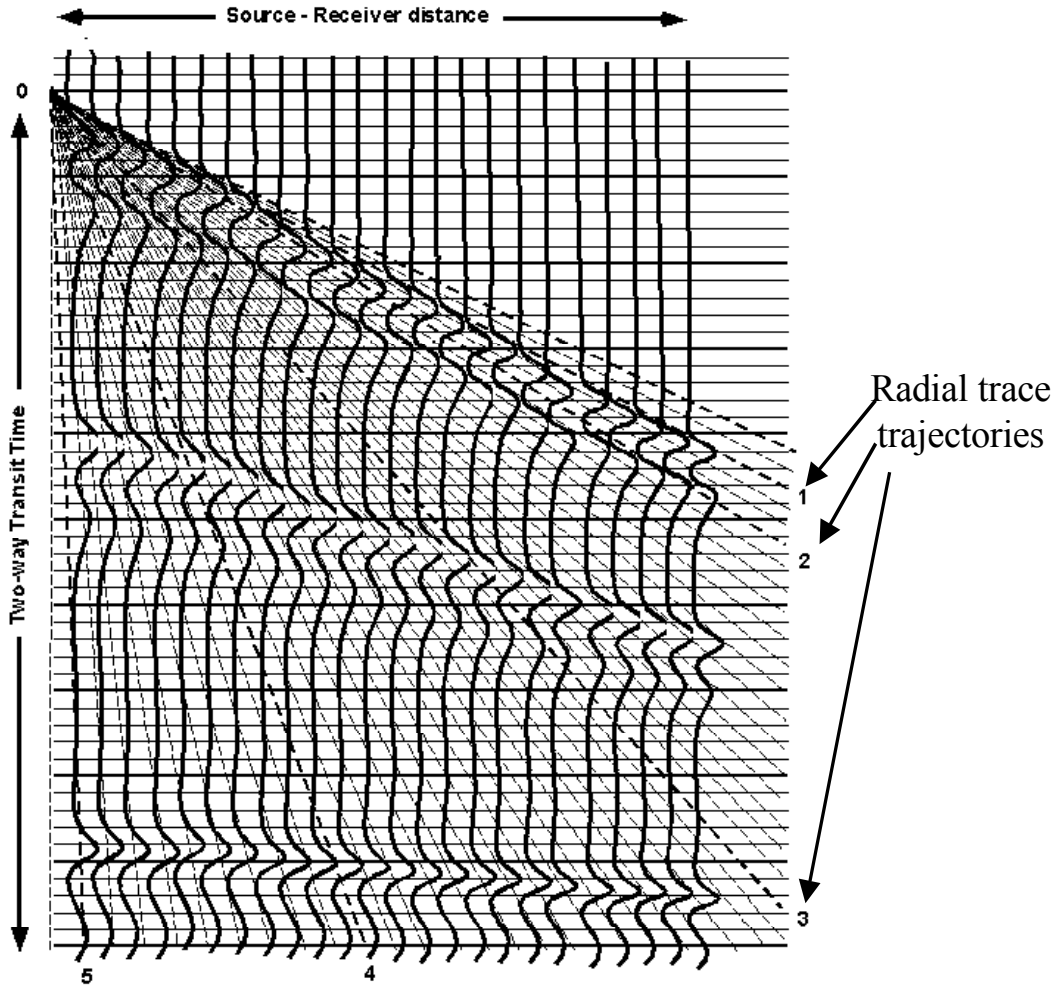

Figure 1 -- Schematic showing the mapping of seismic traces from the X-T domain to the radial trace (R-T) domain. The numbers label representative radial traces to be shown in figure 2. The mapping for a given radial trace proceeds by following a dipping trajectory from its origin to the edge of the X-T panel, selecting an amplitude value from the X-T panel at every sample time, interpolating from the two nearest X-T traces where necessary. Alternatively, the mapping can be done by interpolating the trace amplitudes along lines of constant sample interval (time slices) from the X values of the X-T panel (source-receiver offsets) to the X values computed for the suite of radial traces at the same time sample. The latter proves to more computationally efficient in actual practice.

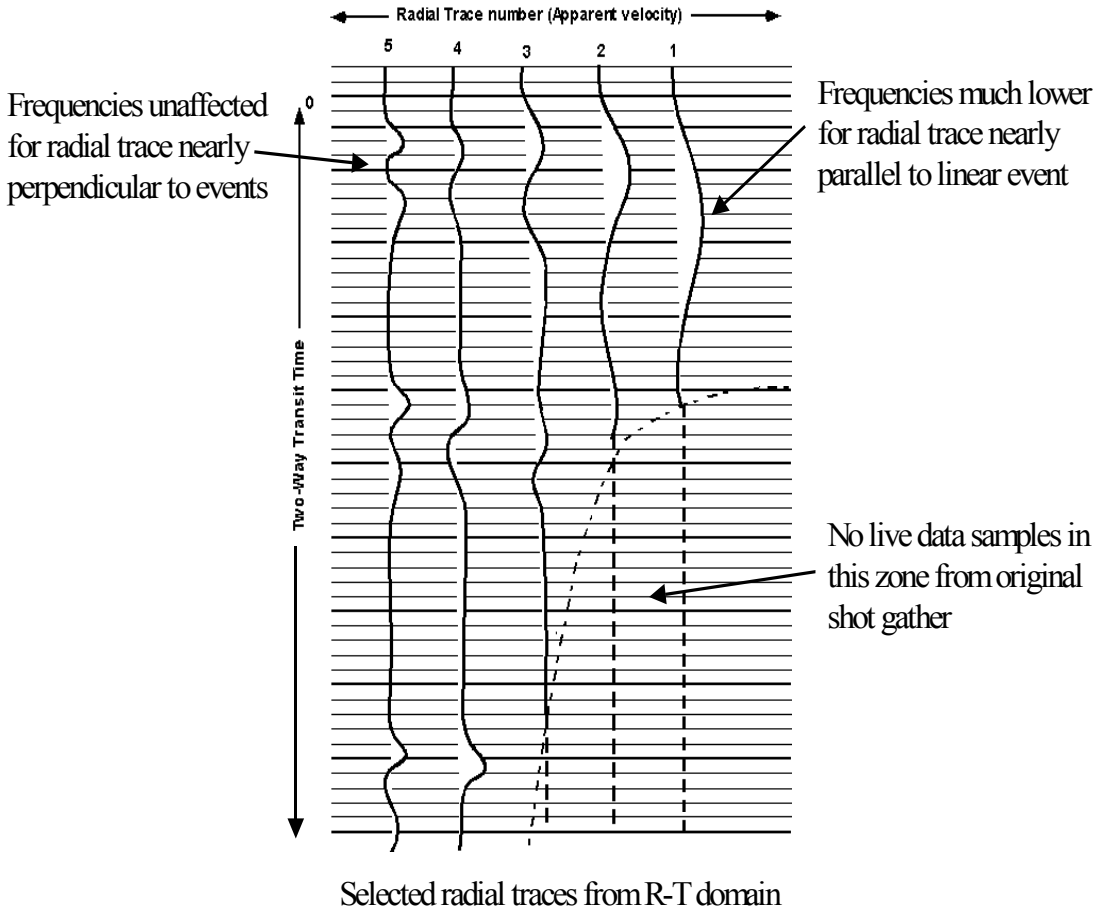

Figure 2 – Schematic showing selected radial traces from the X-T panel in figure 1. Trace numbers correspond to like-numbered trajectories in figure 1. For a high velocity trajectory like no 1, the corresponding radial trace is shorter because the trajectory encounters fewer live samples on the X-T panel before going off the edge of the live data. Low velocity trajectories like no 5, however, span the entire record time of the X-T panel. Because the high velocity trajectories encounter the linear events on the X-T panel very nearly parallel to wavefronts, these linear events are represented on the corresponding radial traces as very low-frequency events—a radial trace perfectly aligned with a linear event would record only a DC level. This shift of apparent frequency in the radial trace domain is what enables coherent noise attenuation and wavefield separation.

Figure 3 – Typical raw shots from the Blackfoot 20m vertical component data set. Linear noise is prominent over much of these records.

Figure 4 – Shot gathers from figure 3 after one pass R-T domain filtering with a low-cut of 15 Hz. Reflections show more continuity, and "back-scatter" noise can now be seen.

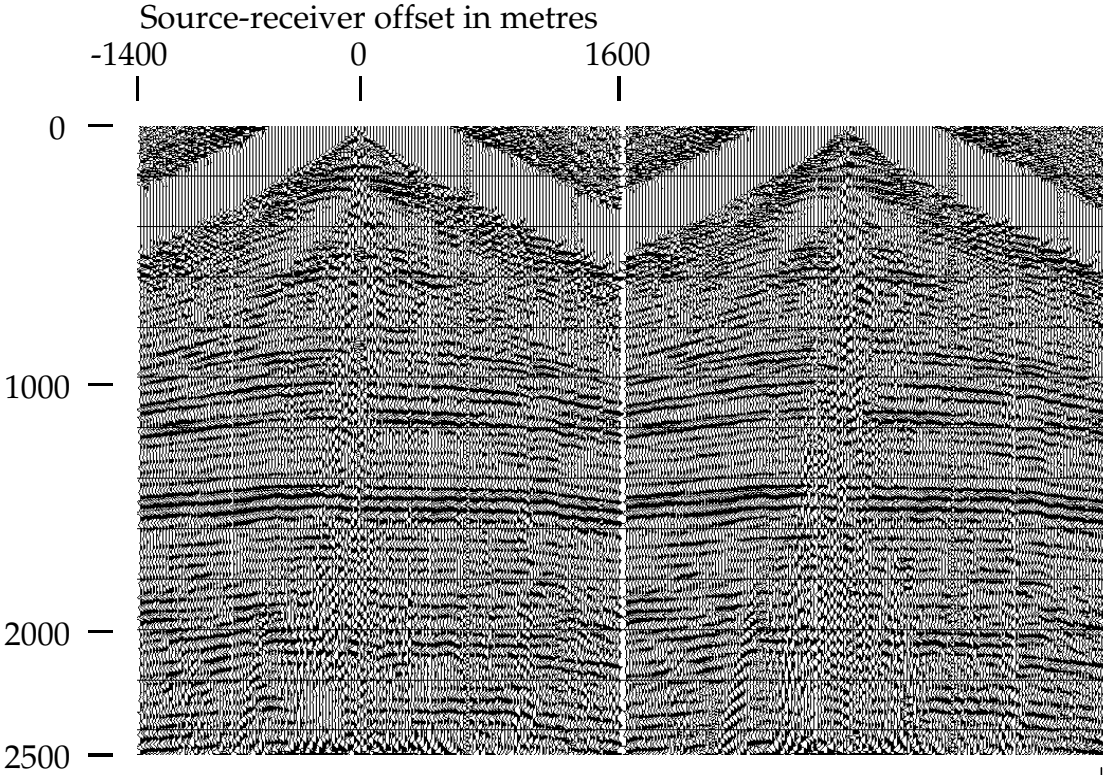

Figure 5 – Blackfoot shots after second pass of R-T filter, this one time-reversed. Much of the back-scatter has been removed, the reflections are more continuous.

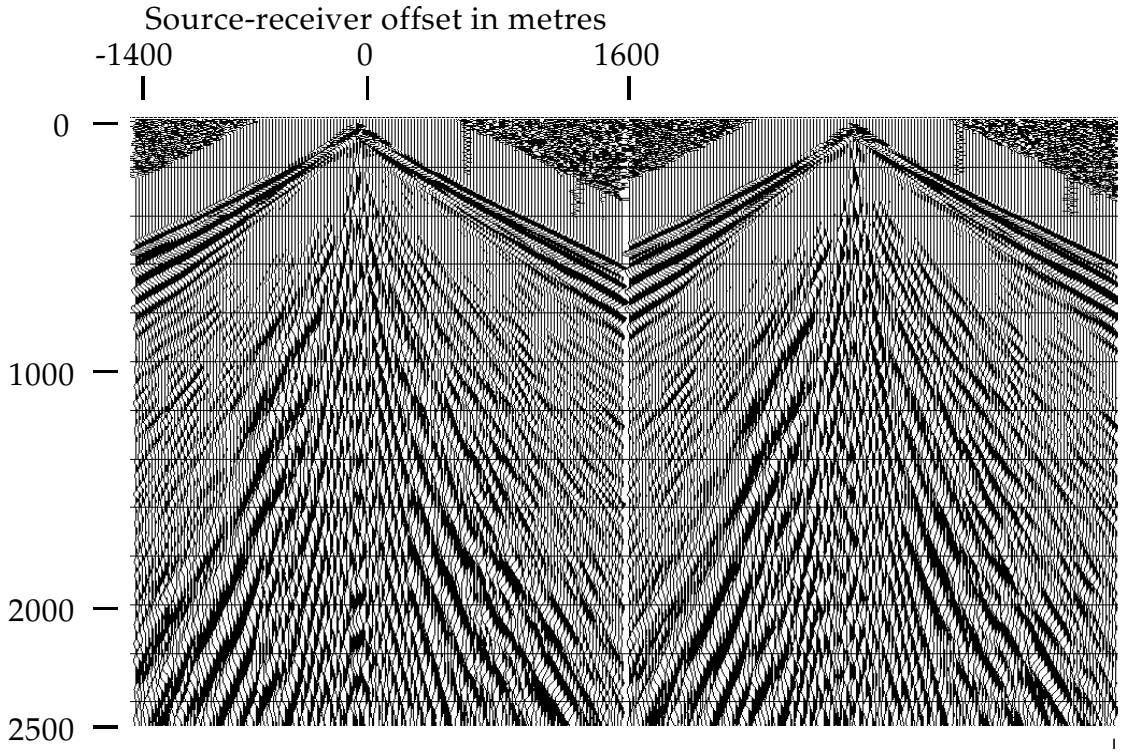

Figure 6 – Blackfoot shots low-pass filtered in the R-T domain. This is essentially the coherent noise filtered out by one low-cut R-T fan filter pass.

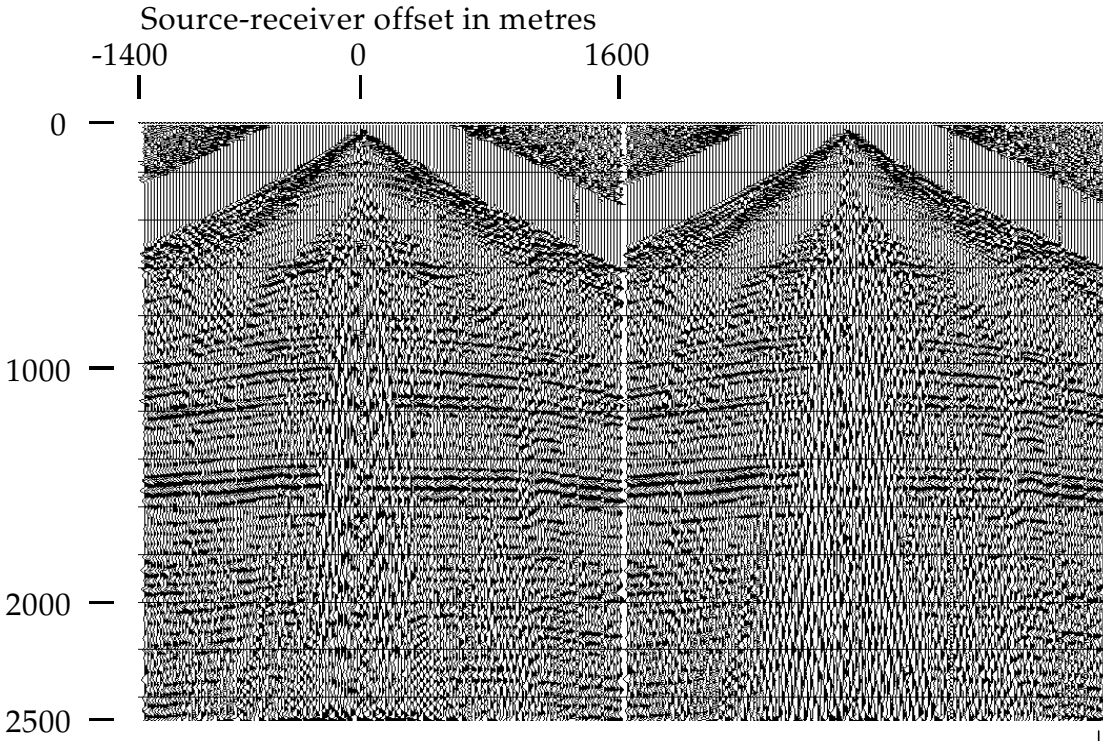

Figure 7 – Result of subtracting the noise estimated in figure 6 from the raw shots in figure 3. The results are not as good as a straightforward low-cut R-T fan filter pass.

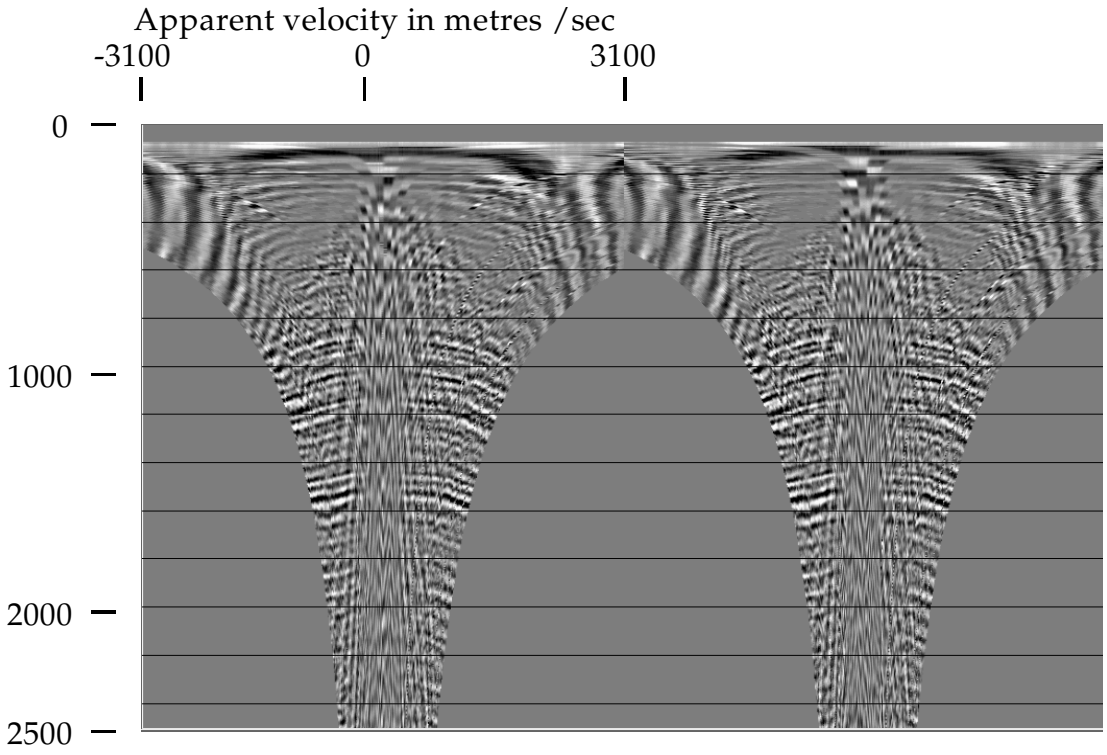

Figure 8 – The raw shots of figure 1 in the R-T domain. Near-vertical bands of energy correspond to linear noises mapped into the R-T domain.

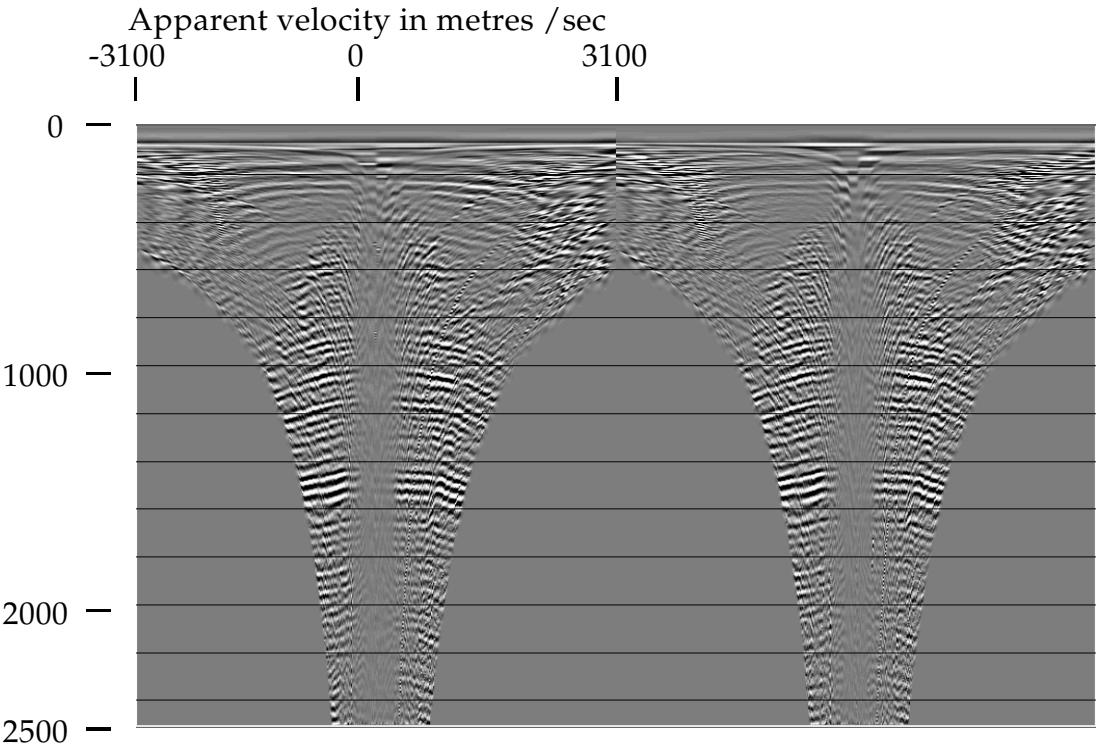

Figure 9 – R-T domain traces after application of low-cut filter. Traces were not re-normalized, so that comparison to figure 8 will show the energy removed by the filter.

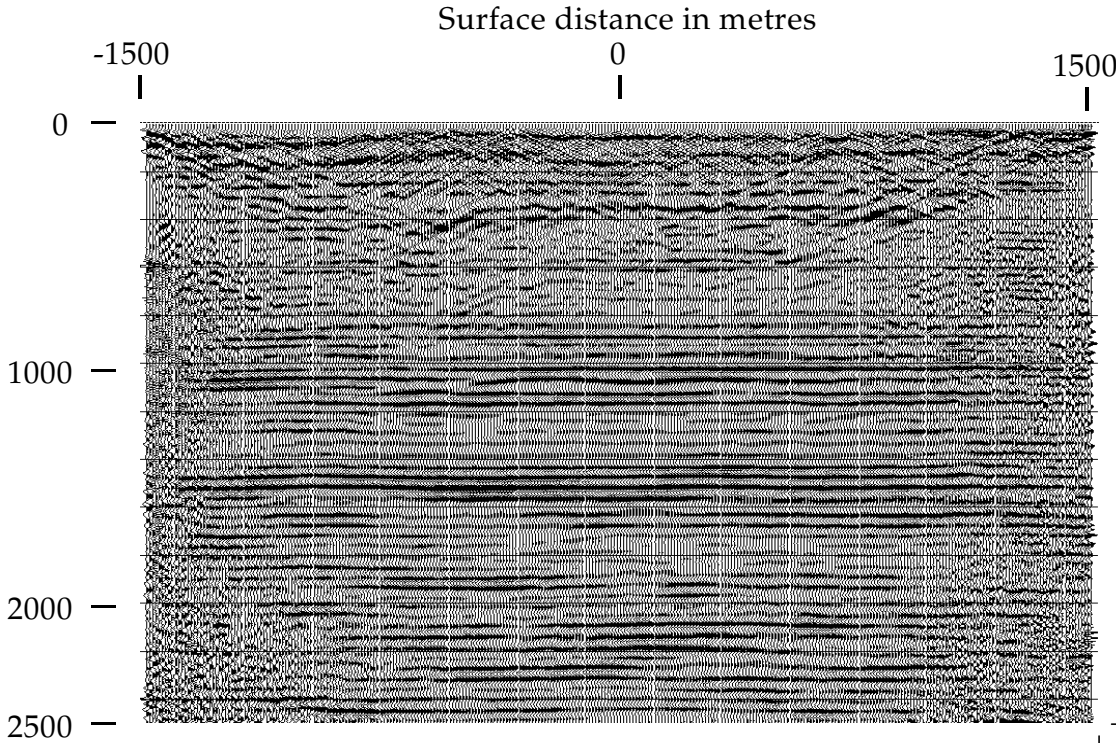

Figure 10 – Brute CDP stack of shot gathers low-cut filtered at 15 Hz. in the X-T domain. This is the baseline standard for judging the effectiveness of R-T domain filtering.

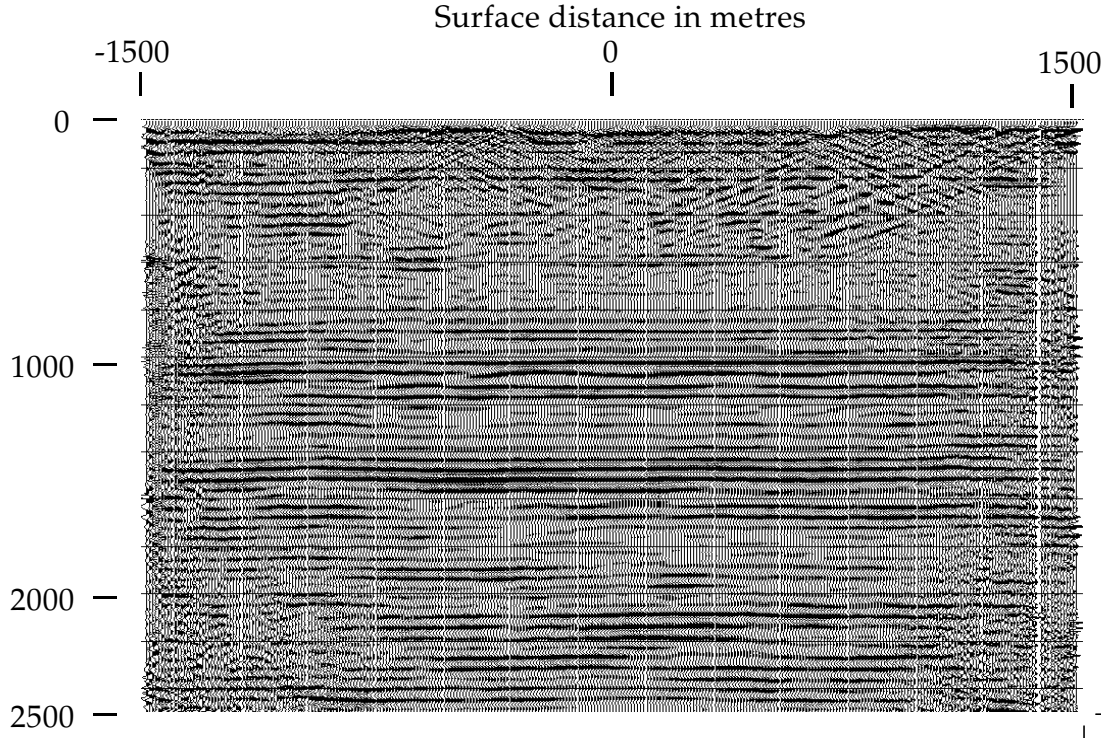

Figure 11 – Stack of shot gathers which have been low-cut filtered in the R-T domain at 15 Hz. The most improvement with respect to figure 10 is in the shallow portion of the section.

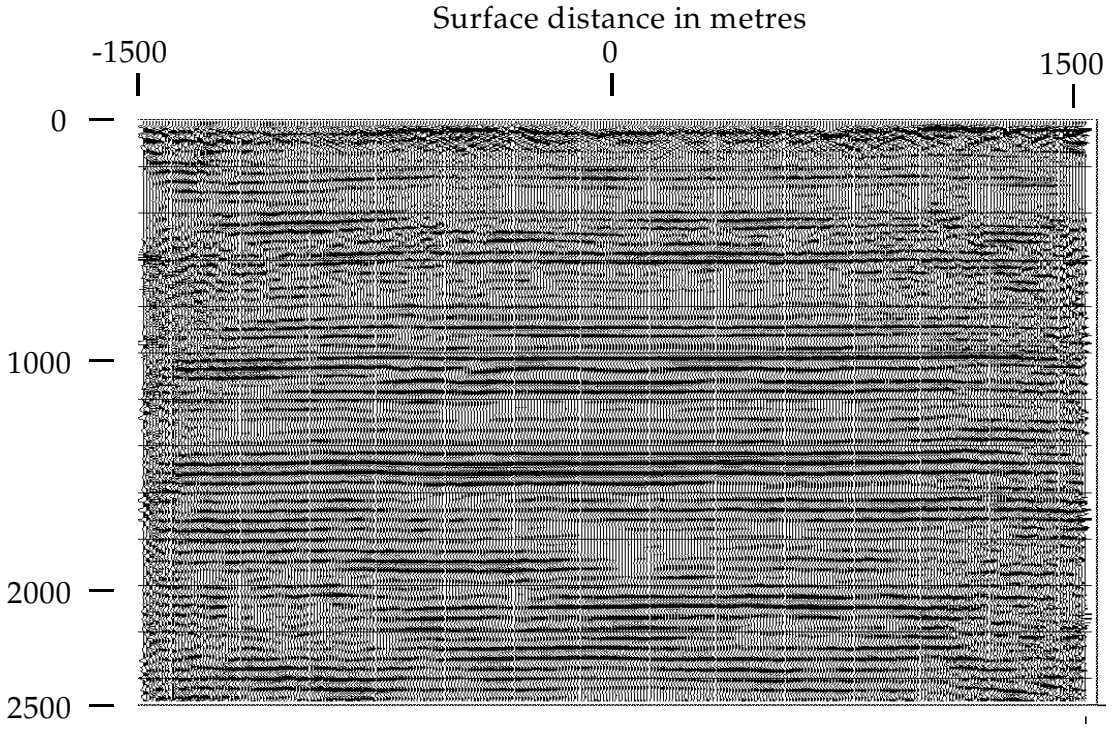

Figure 12 – Blackfoot CDP stack in which the shot gathers have been filtered twice in the R-T domain (one pass inverted) and the receiver gathers once. The section is significantly improved, but residual dipping noise can be seen upon close inspection.

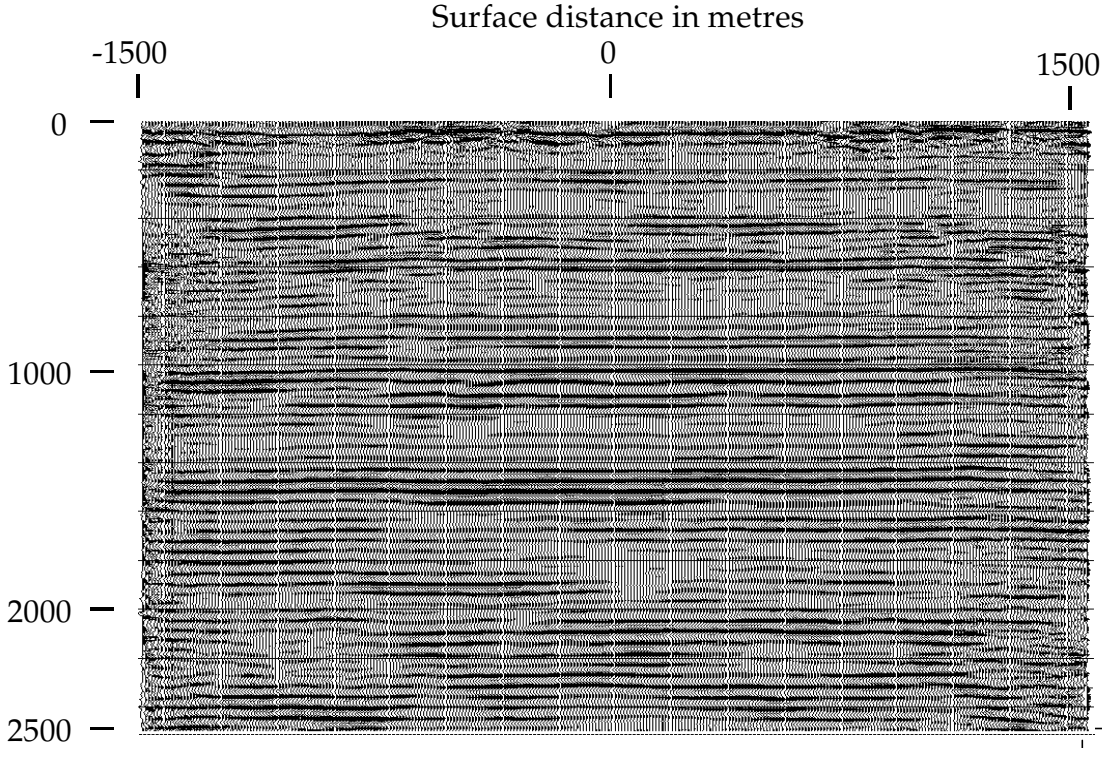

Figure 13 – Stack of figure 12 after the application of post-stack R-T domain dip filters. Dipping noise is further attenuated.

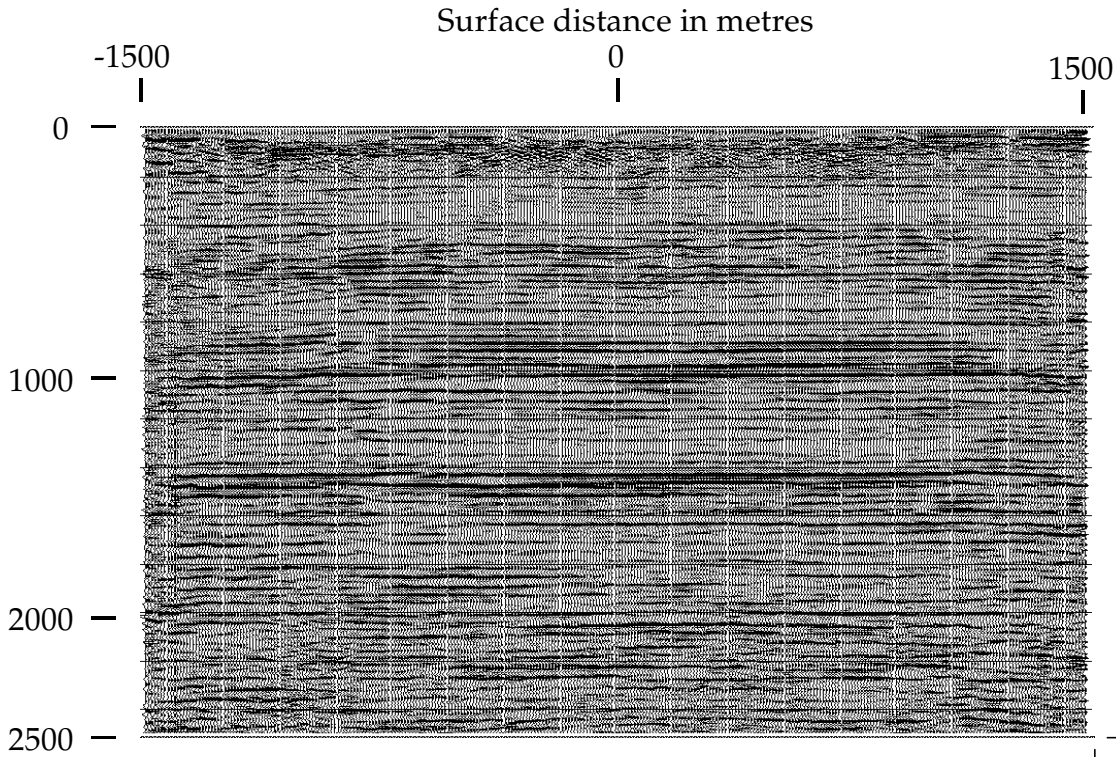

Figure 14 – Section of figure 13 after application of mild predictive deconvolution and F-X deconvolution. These steps restore higher frequencies to the section.

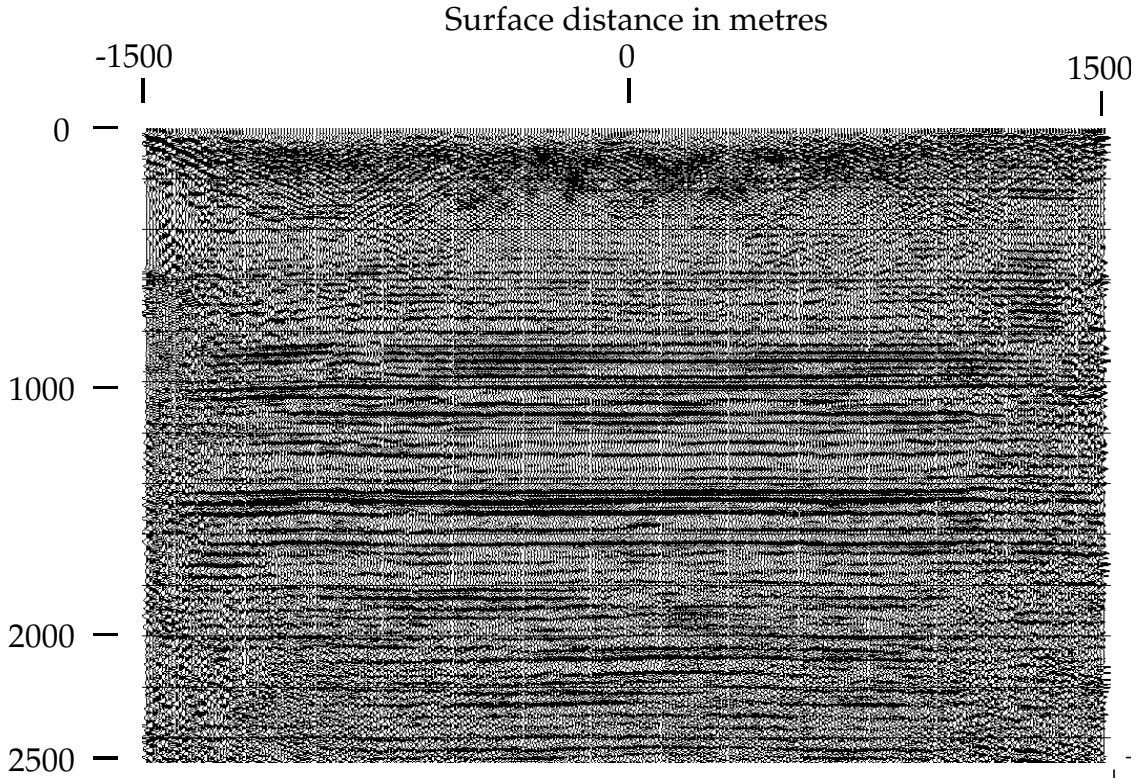

Figure 15 – Blackfoot brute stack from figure 10 after application of post-stack predictive deconvolution and F-X deconvolution to restore higher frequencies. Differences between this section and that in figure 14 are now quite evident.

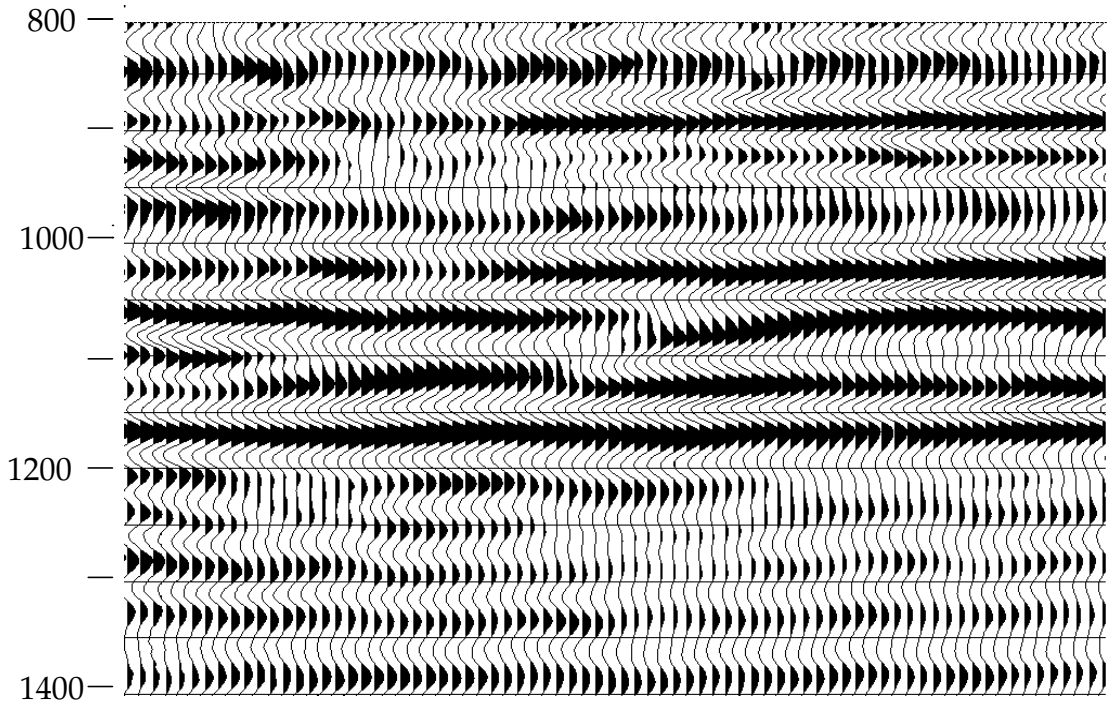

Figure 16 – A channel feature as it appears on the brute stack section.

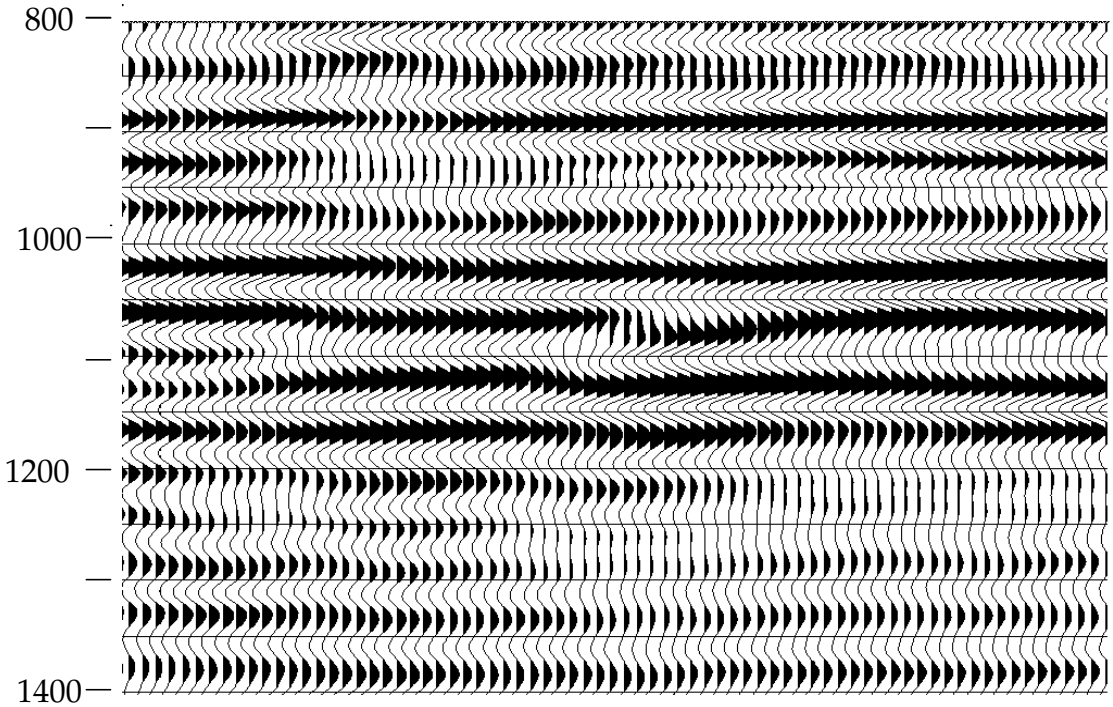

Figure 17 – Channel feature as it appears on the section whose shots have been R-T filtered twice, receiver gathers once; and which has been post-stack R-T dip filtered. Differences between this figure and the previous one are relatively minor.

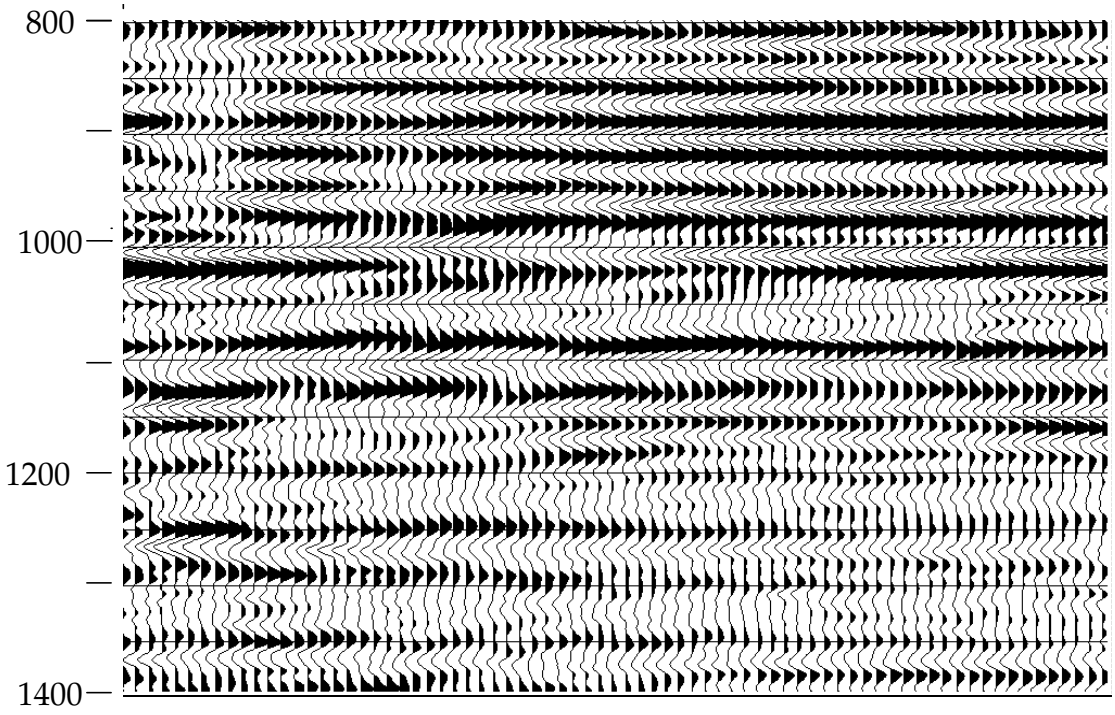

Figure 18 – Channel feature after pre- and post-stack R-T filtering, post-stack deconvolution.

Figure 19 – Channel feature as seen on the post-stack deconvolved brute stack. The appearance is quite different from figure 18, which could influence interpretation.

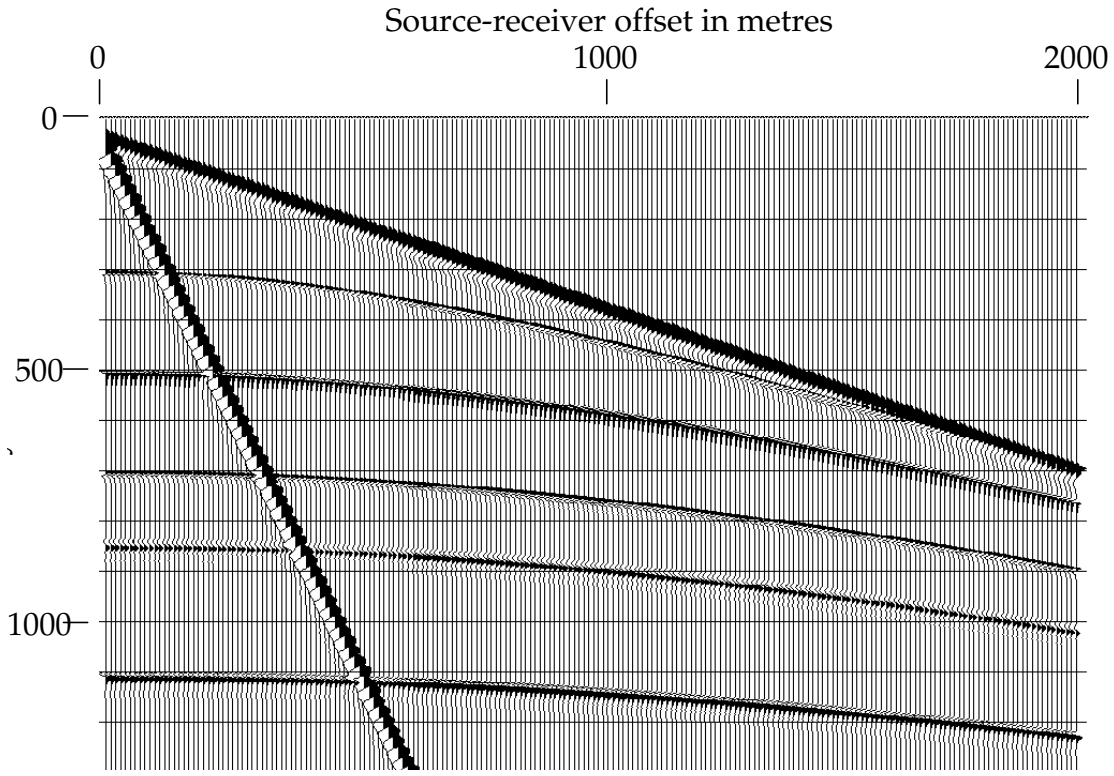

Figure 20 – Synthetic shot gather created to test R-T domain and F-K domain filters. Linear "noise" events are significantly stronger than the hyperbolic "reflections".

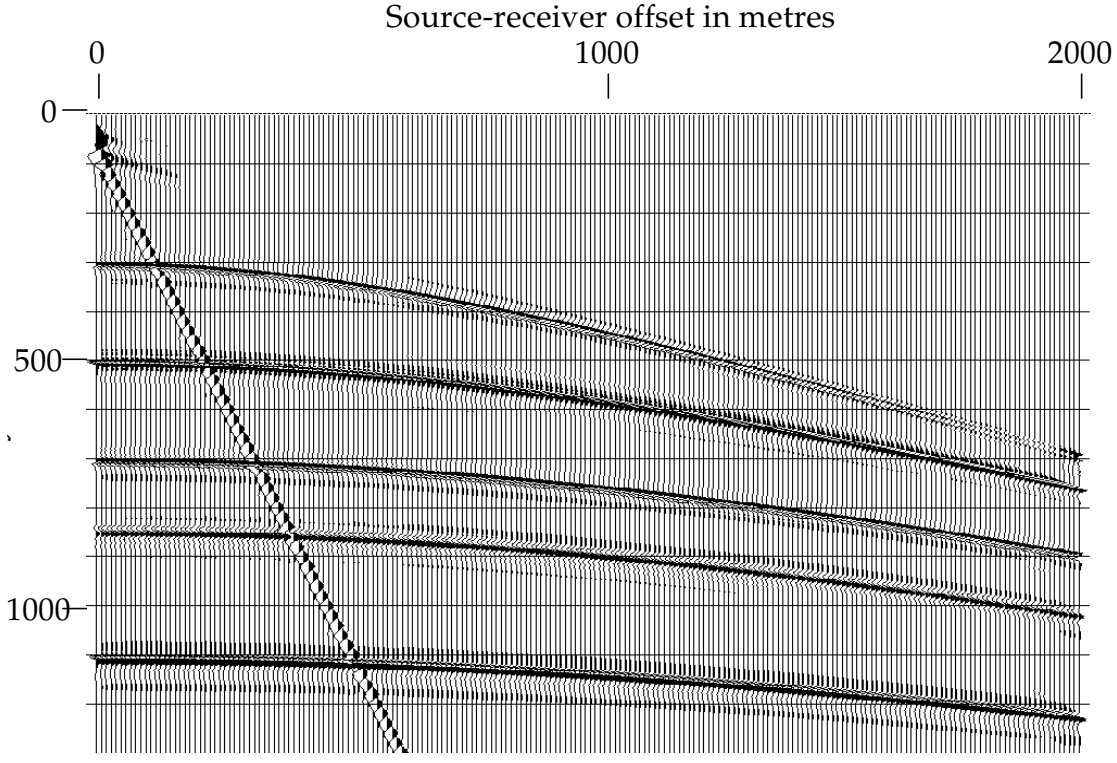

Figure 21 – Synthetic shot gather after application of typical R-T fan filter. Fast linear event is nearly gone, while slow event is significantly attenuated.

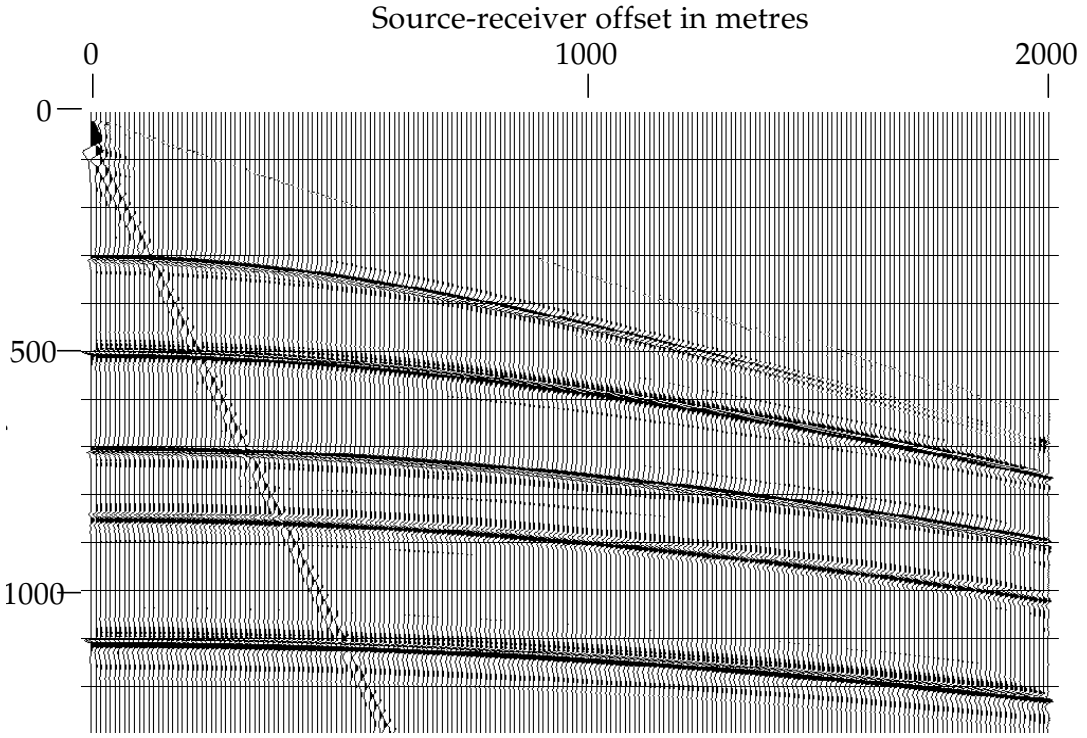

Figure 22 – Synthetic shot gather after application of a second R-T fan filter with origin chosen to coincide with that of slow linear event, which is additionally attenuated.

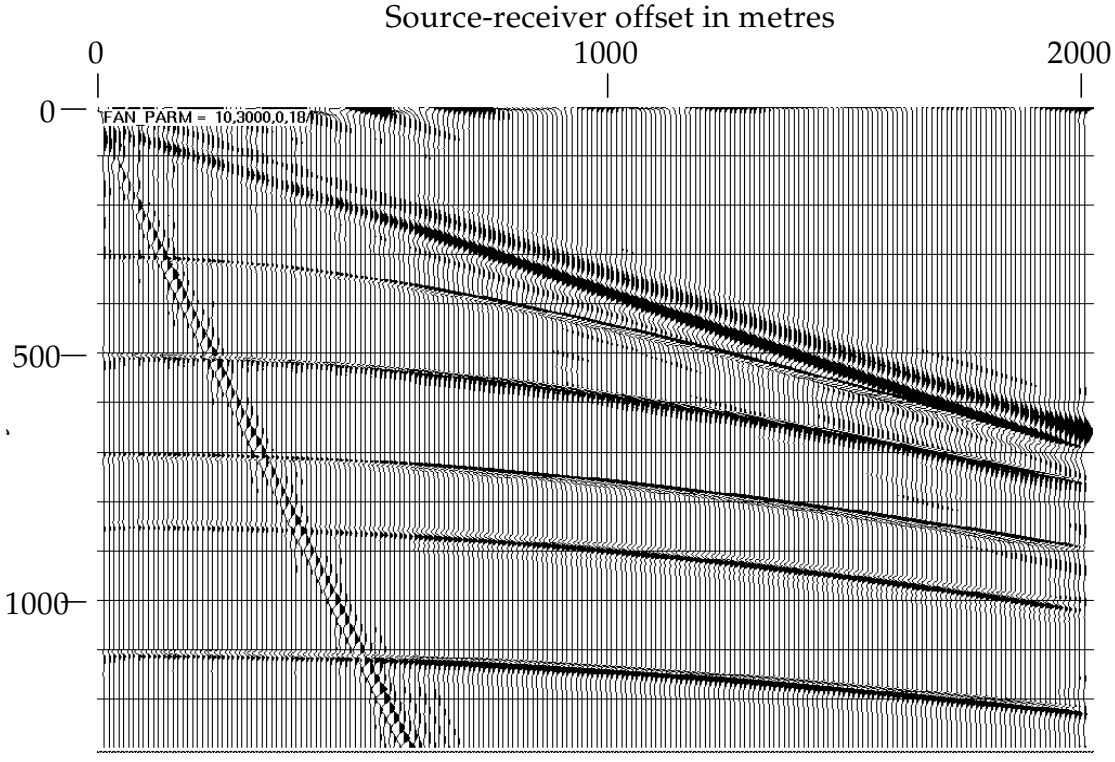

Figure 23 – Synthetic shot gather after application of F-K velocity reject filter. Gather traces have not been re-normalized after filter application. Both linear events attenuated somewhat.

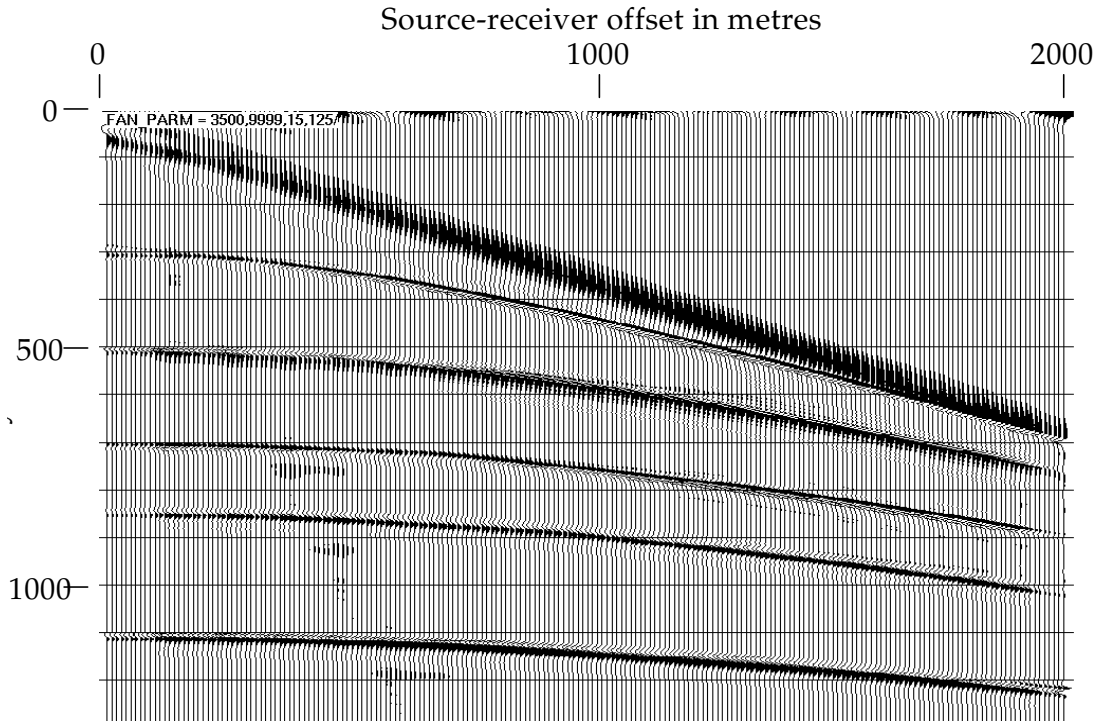

Figure 24 – Synthetic shot gather after application of F-K velocity boost filter. Gather traces have not been re-normalized after the filter. Low velocity event has been nearly totally removed. High velocity event attenuated.

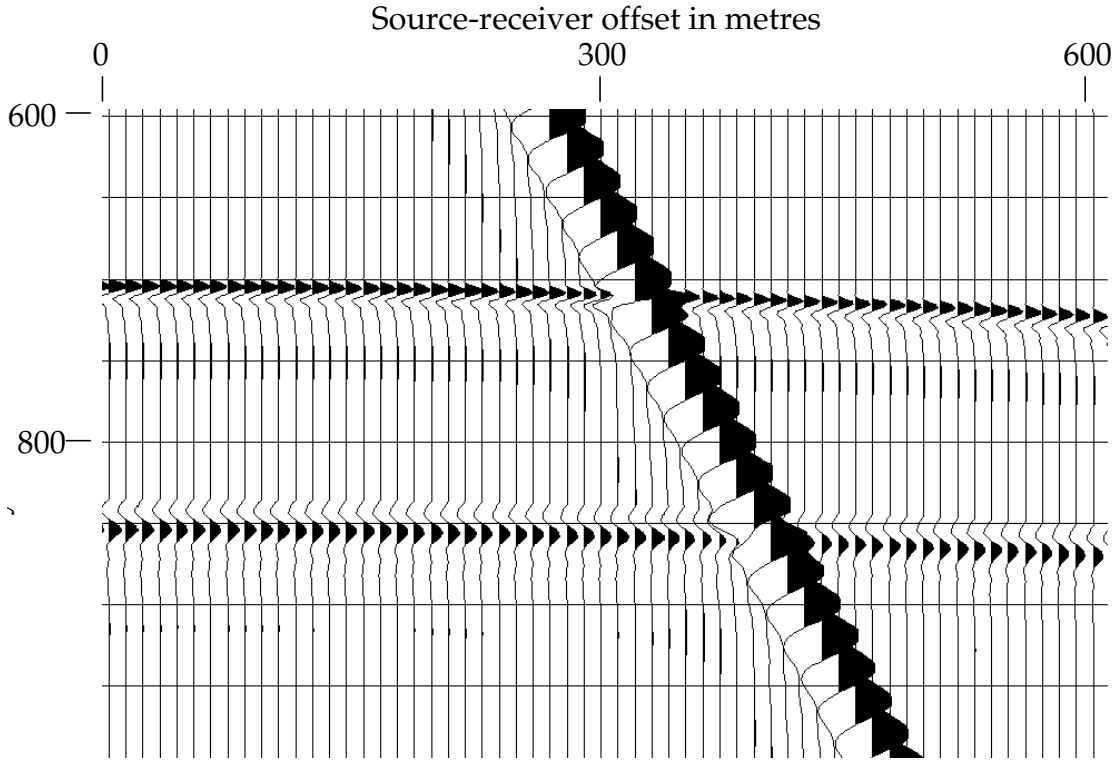

Figure 25 – Detail of the synthetic gather in figure 20. Note strength and apparent frequency of low velocity linear event with respect to “reflections”. This detail in the “low velocity” portion of R-T domain.

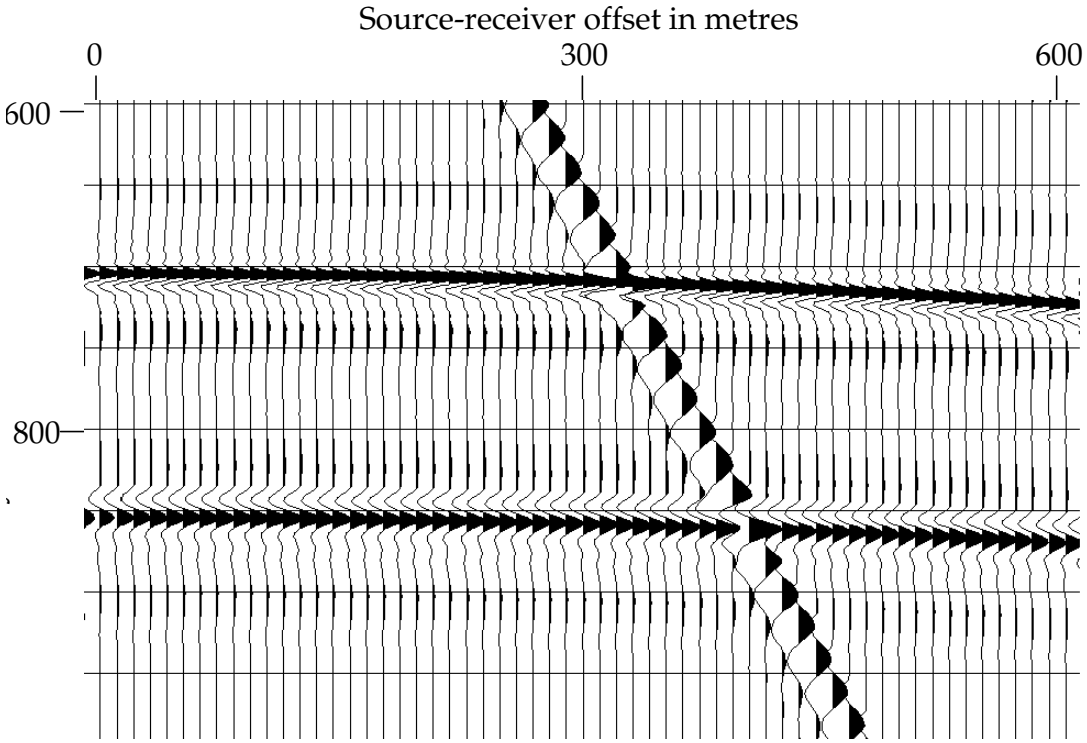

Figure 26 – Detail of the synthetic gather after one pass of R-T domain fan filter.

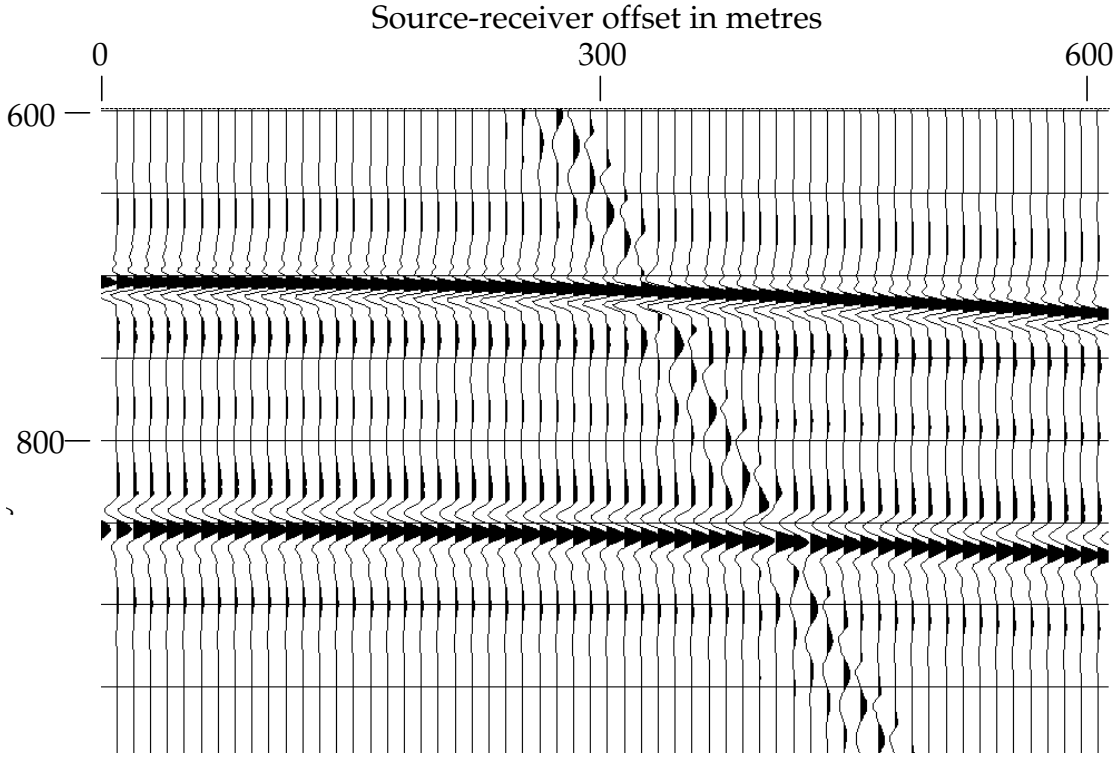

Figure 27 – Detail of synthetic shot gather after two R-T filter passes.

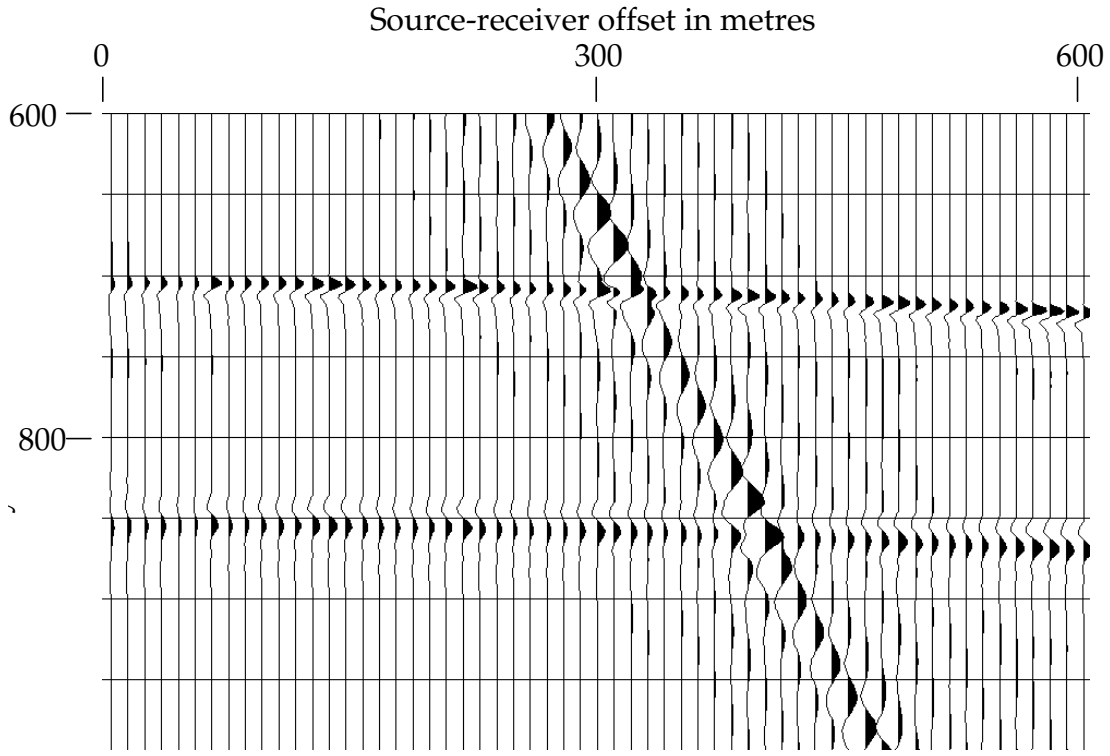

Figure 28 – Detail of synthetic gather after application of F-K velocity reject filter.

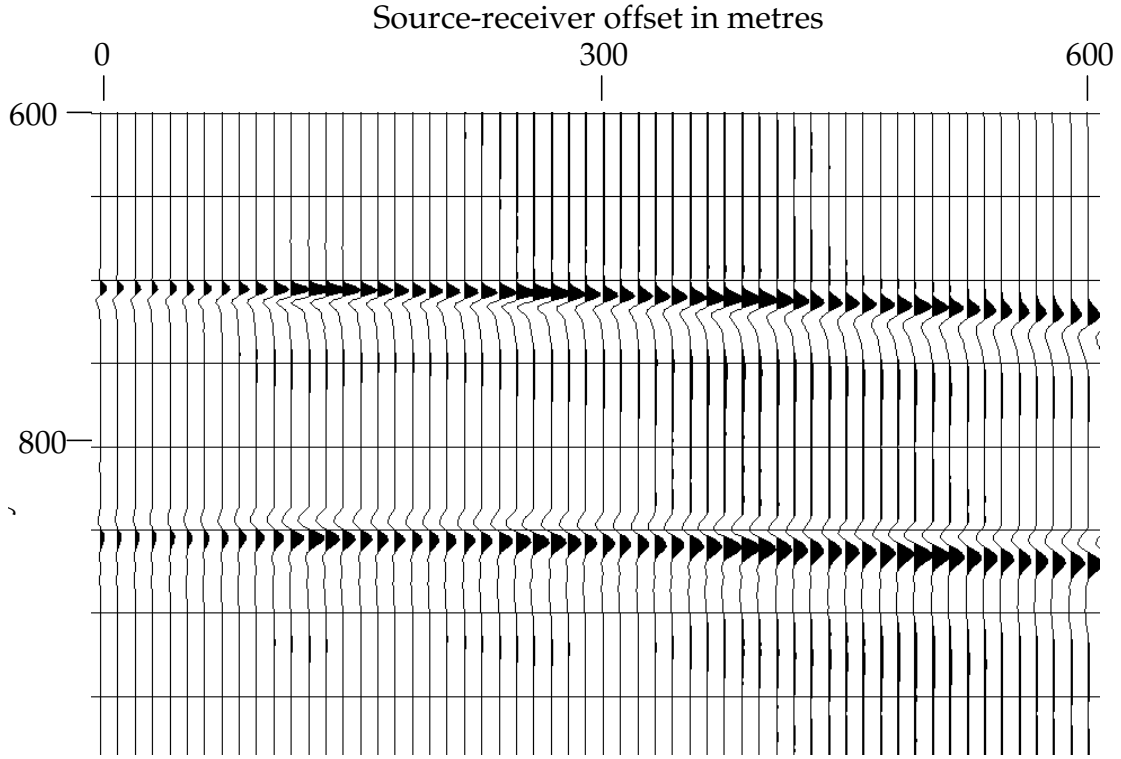

Figure 29 – Detail of synthetic gather after application of F-K velocity boost filter.

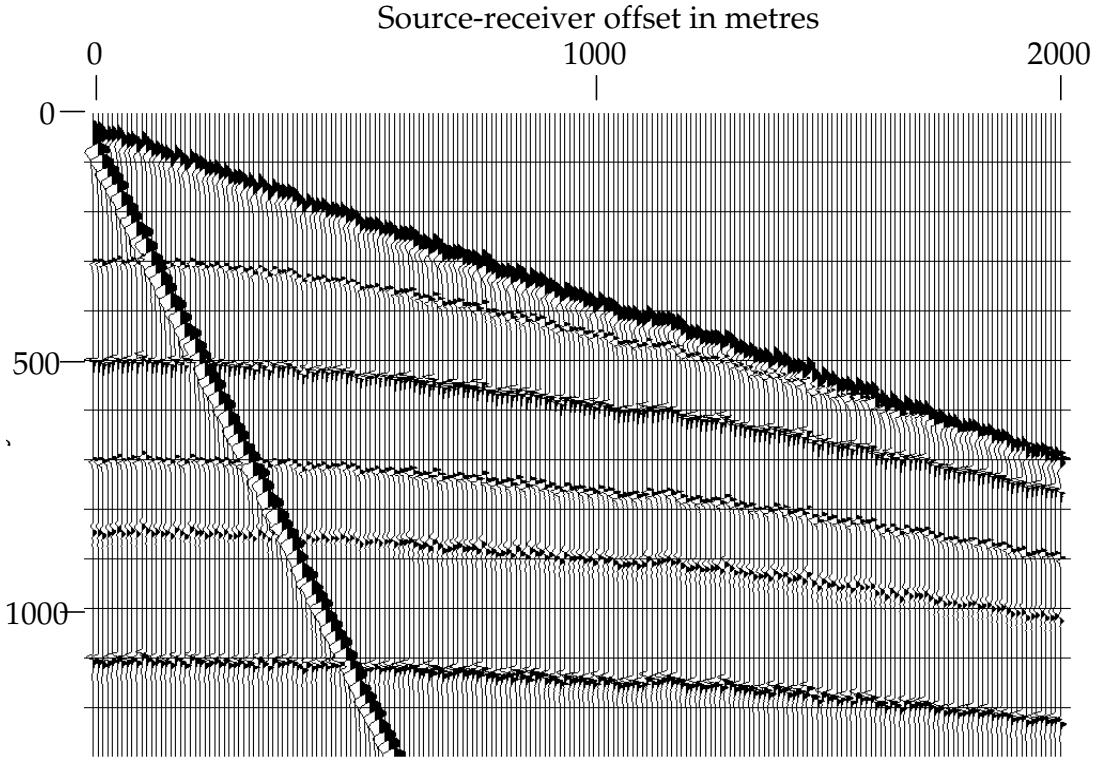

Figure 30 – Synthetic gather of figure 20 after the application of pseudo-random static shifts to the traces. Shifts affect the linear events as well as the reflections.

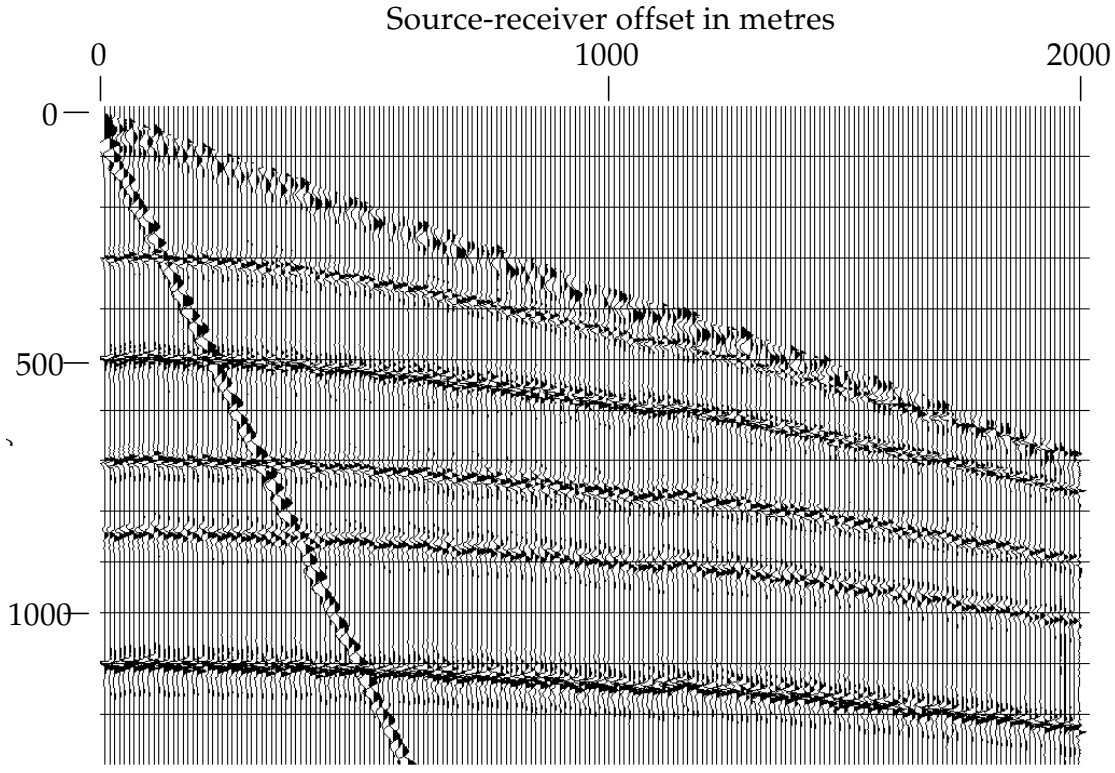

Figure 31 – Synthetic gather with statics after application of one pass of R-T fan filter. Noise attenuation somewhat diminished, but static shifts survive.

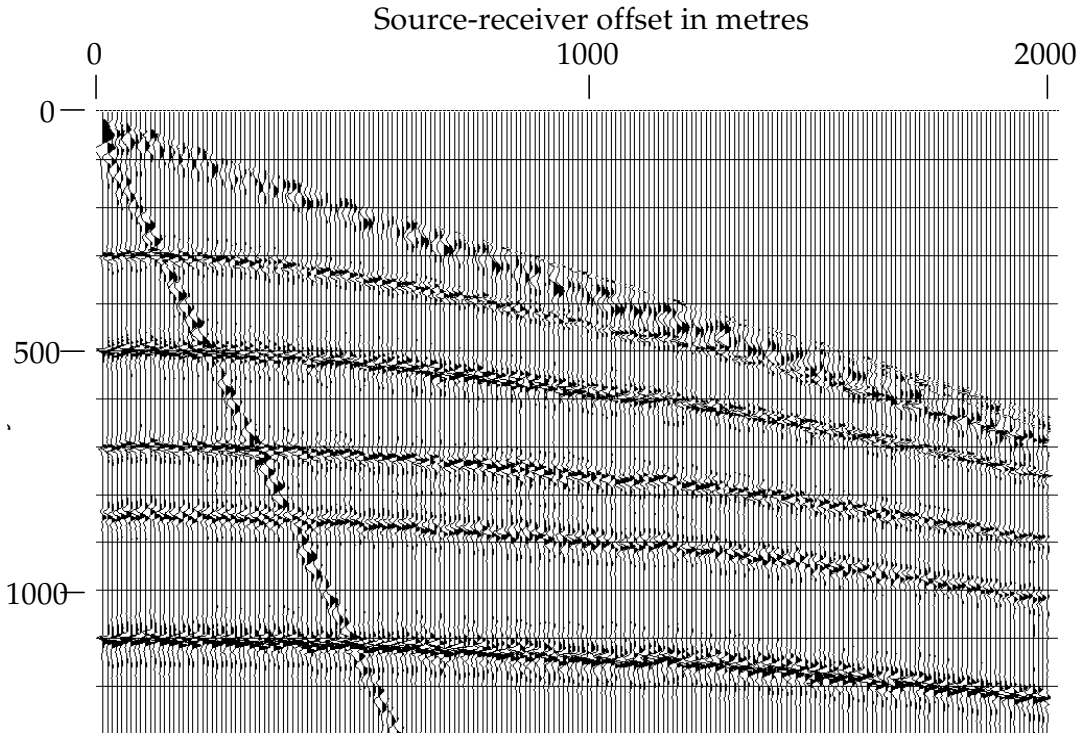

Figure 32 – Synthetic gather with statics after application of two passes R-T fan filter. Attenuation improved, static shifts still survive.

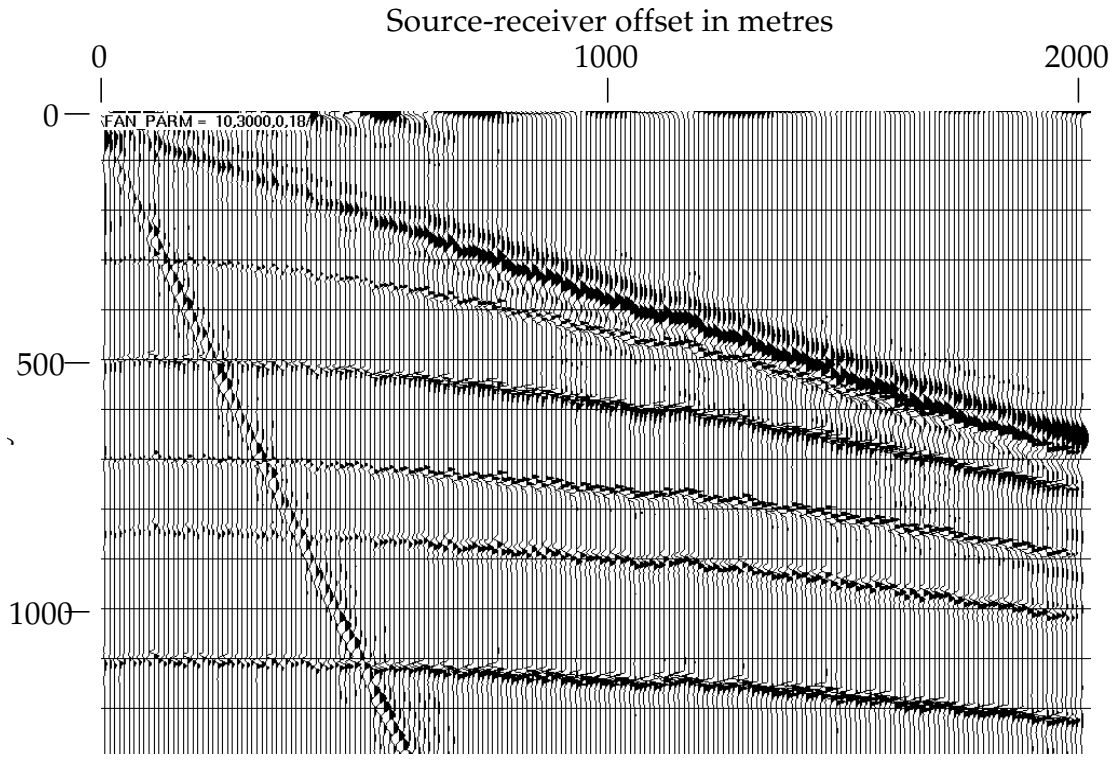

Filter 33 – Synthetic gather with statics after application of F-K velocity reject filter. Static shifts are very well preserved, noise attenuation is moderate.

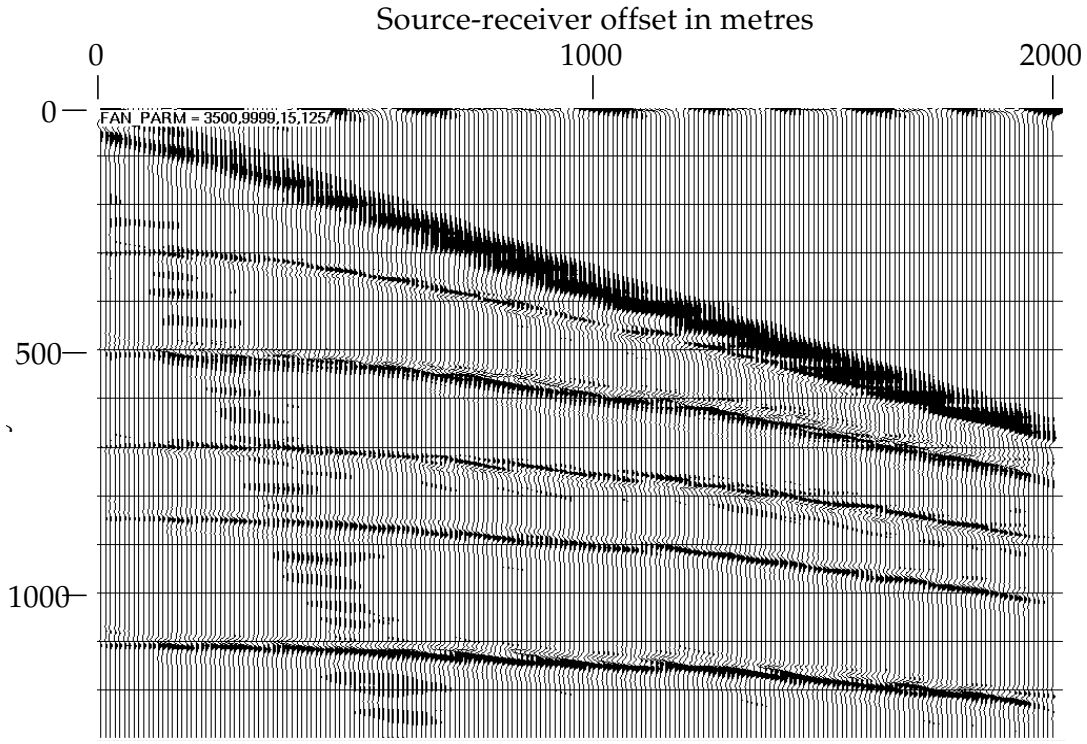

Figure 34 – Synthetic gather with statics after application of F-K velocity boost filter. Static shifts are completely smeared, and the low velocity linear event is less effectively attenuated.

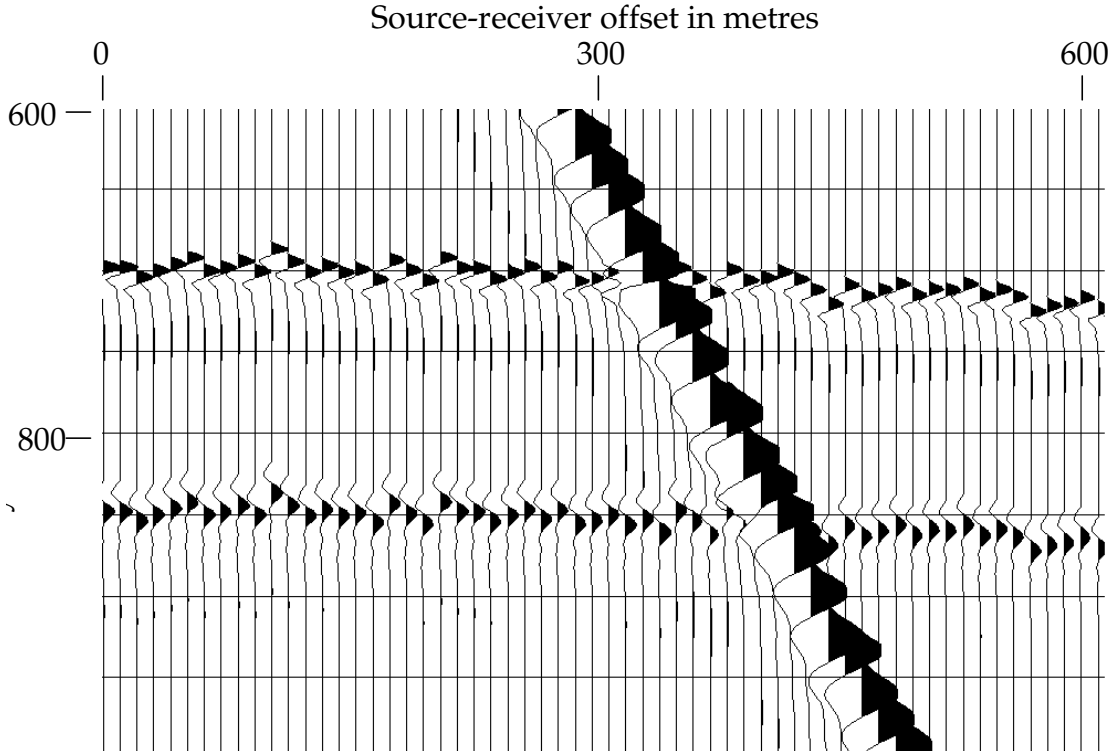

Figure 35 – Detail of synthetic gather with pseudo-random statics applied.

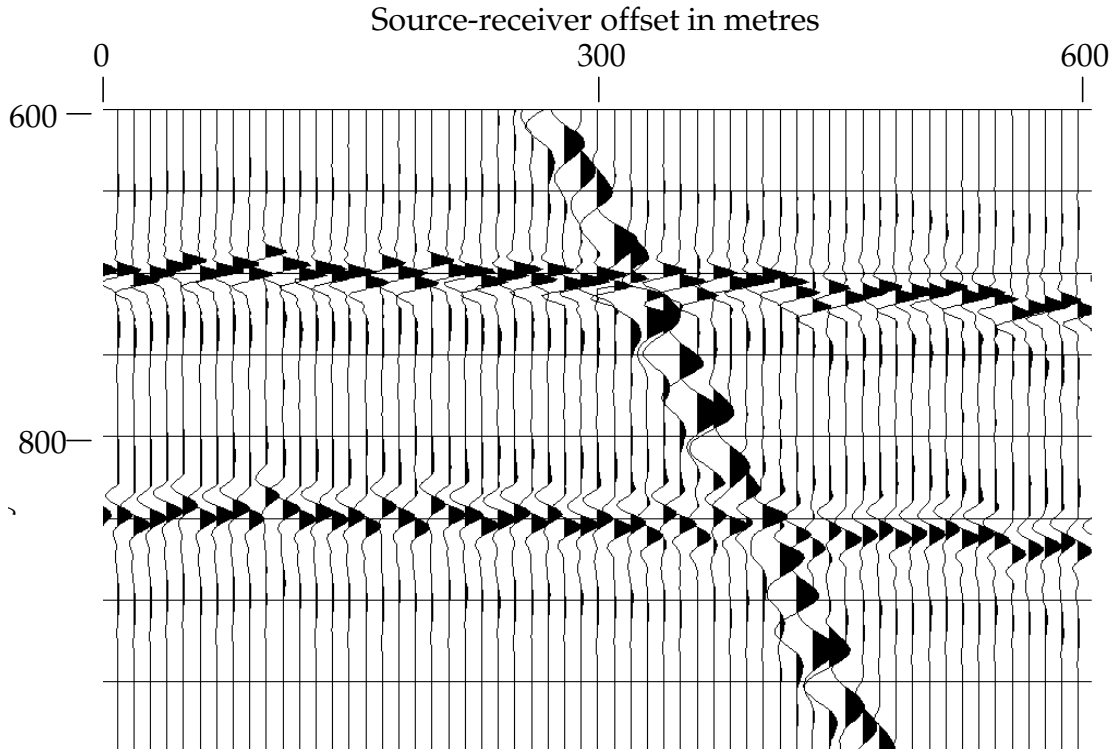

Figure 36 – Detail of synthetic gather with statics after one pass of R-T fan filter.

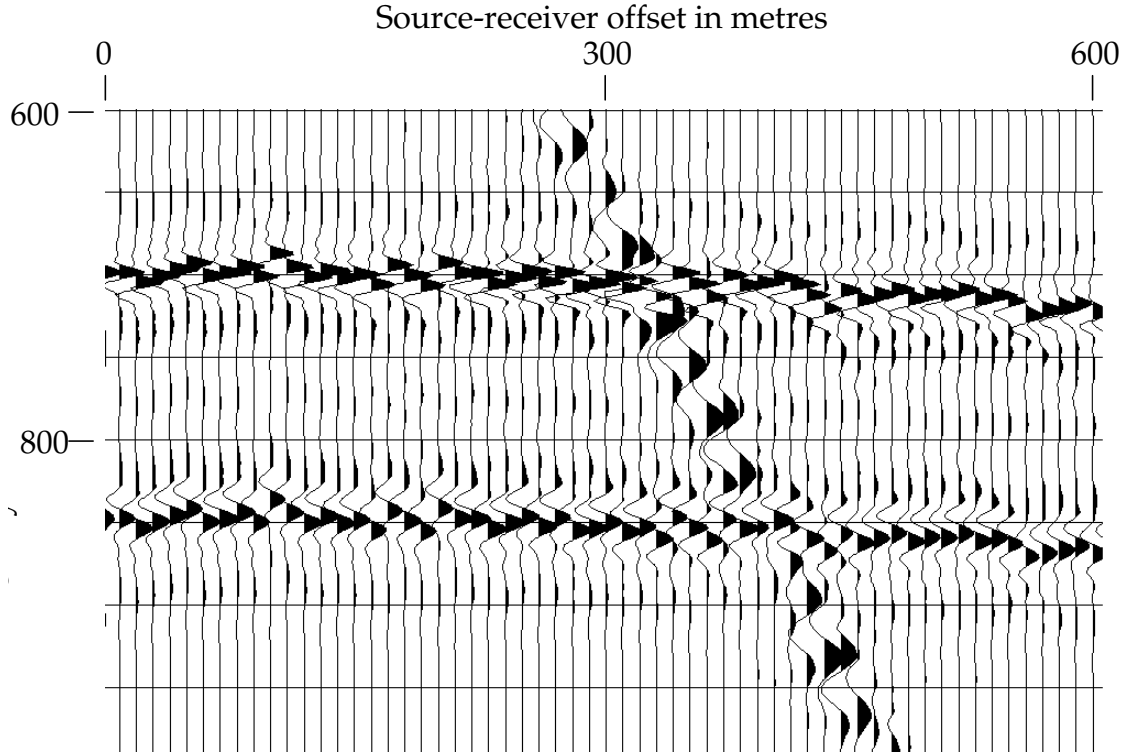

Figure 37 – Detail of synthetic gather with statics after two passes of R-T fan filter. Static shifts are preserved, but filter tails are beginning to fill blank zones.

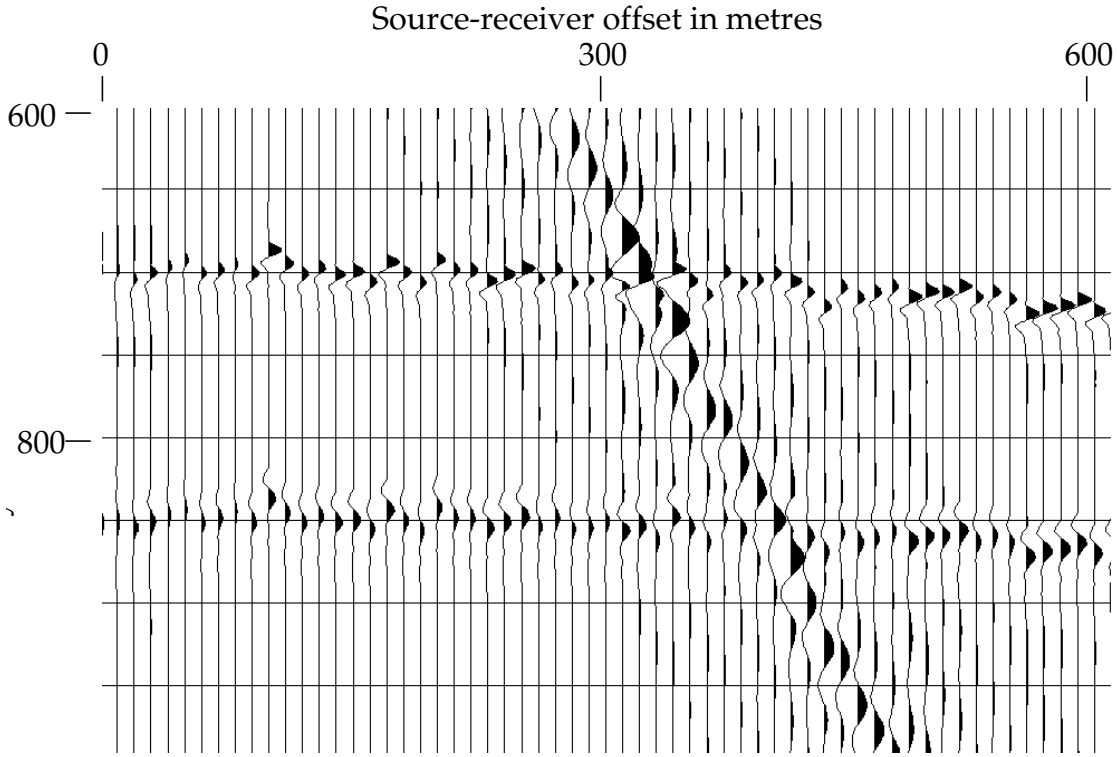

Figure 38 – Detail of synthetic gather with statics after F-K velocity reject filter. Static shifts are preserved, but event amplitudes are disturbed.

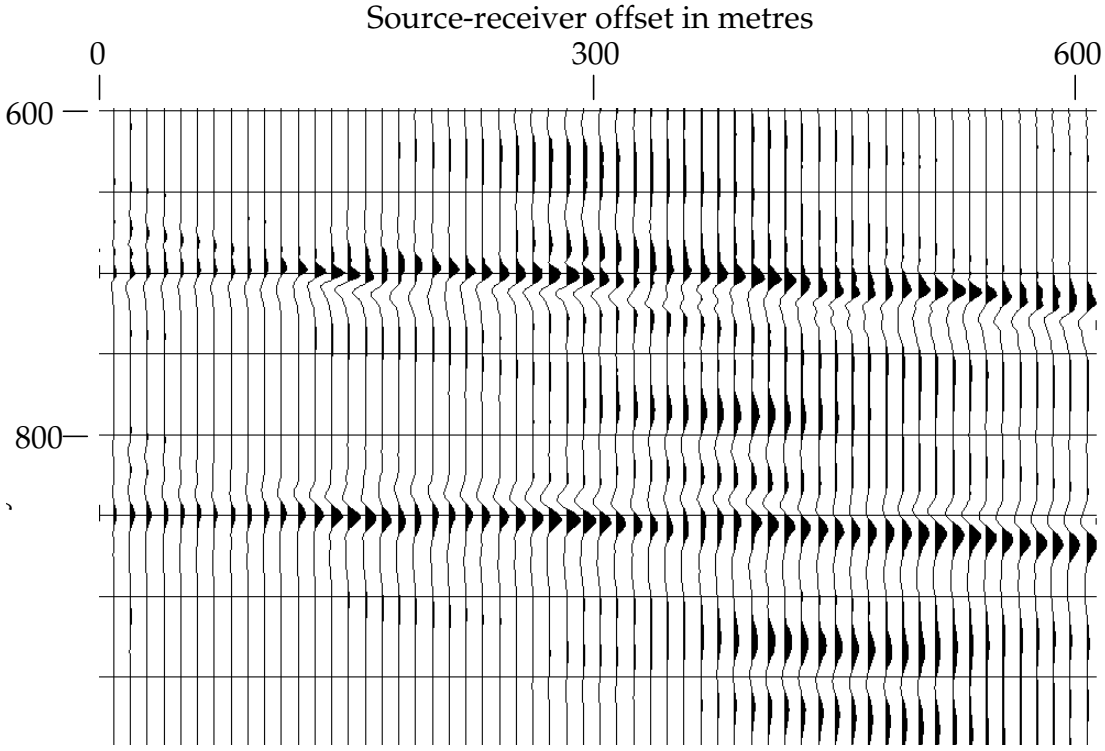

Figure 39 – Detail of synthetic gather with statics after application of F-K velocity boost filter. Static shifts are totally smeared, amplitudes disturbed.

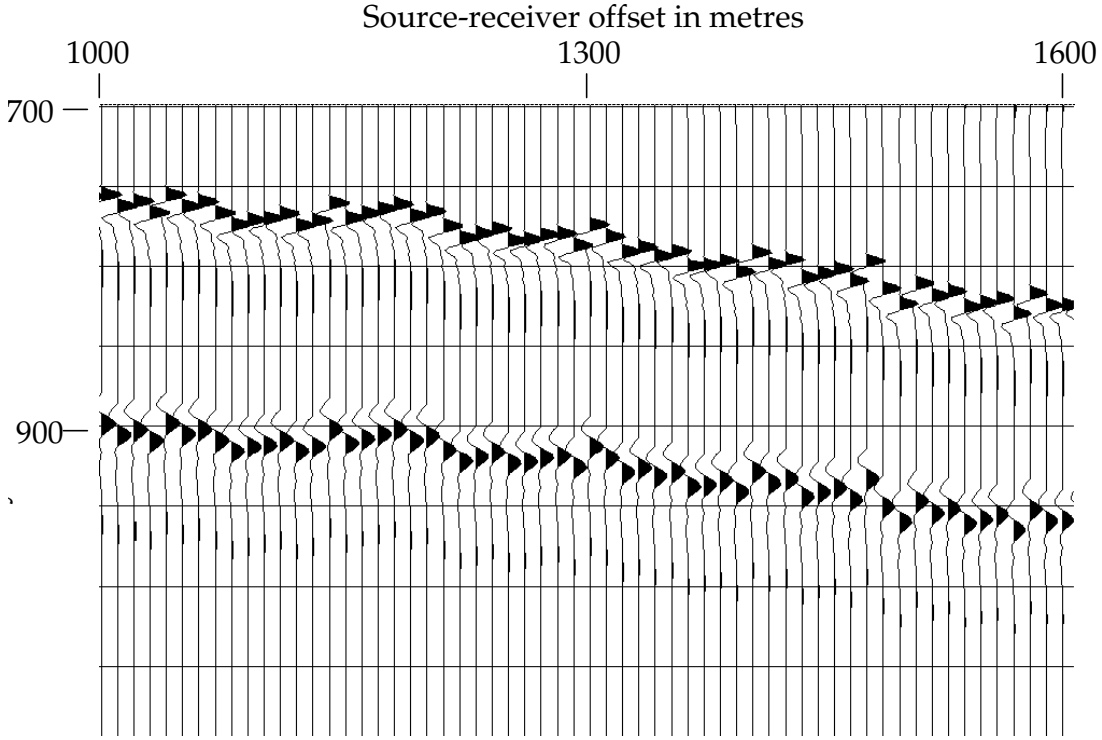

Figure 40 – Detail of synthetic gather with statics at longer offsets, shorter times than previous detail area. This detail is from the “high velocity” zone of the R-T domain.

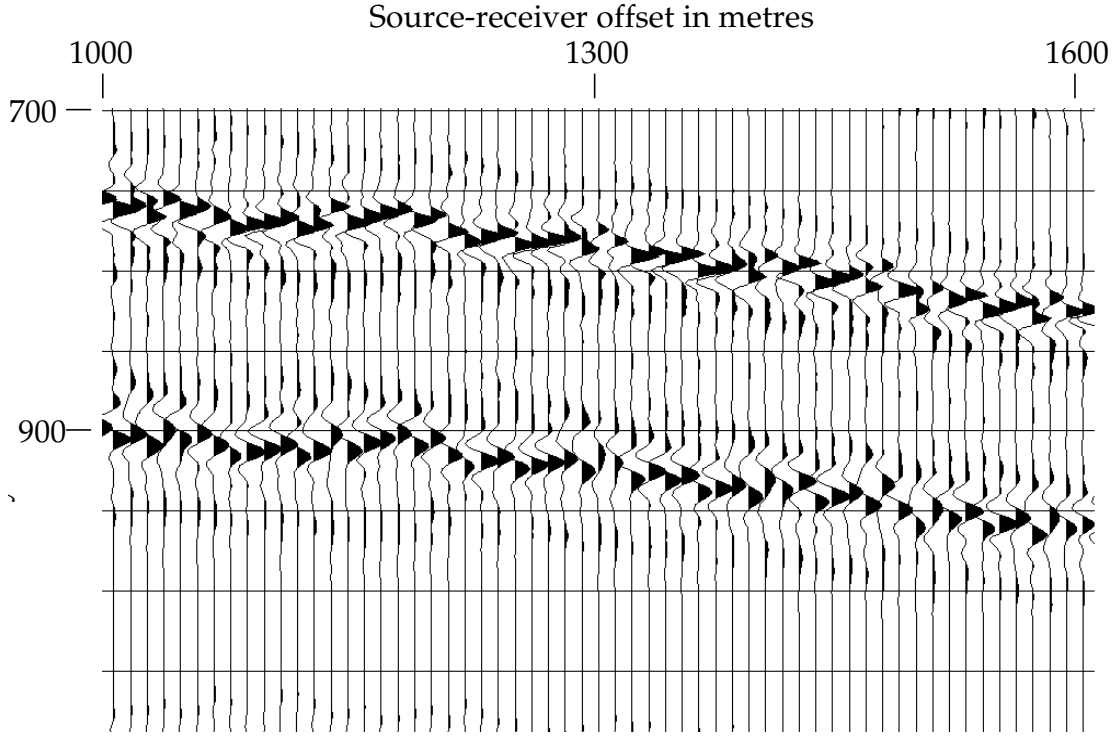

Figure 41 – Detail of synthetic gather with statics from the high velocity portion of the R-T domain after one pass of R-T fan filter. Static shifts mostly well-preserved.

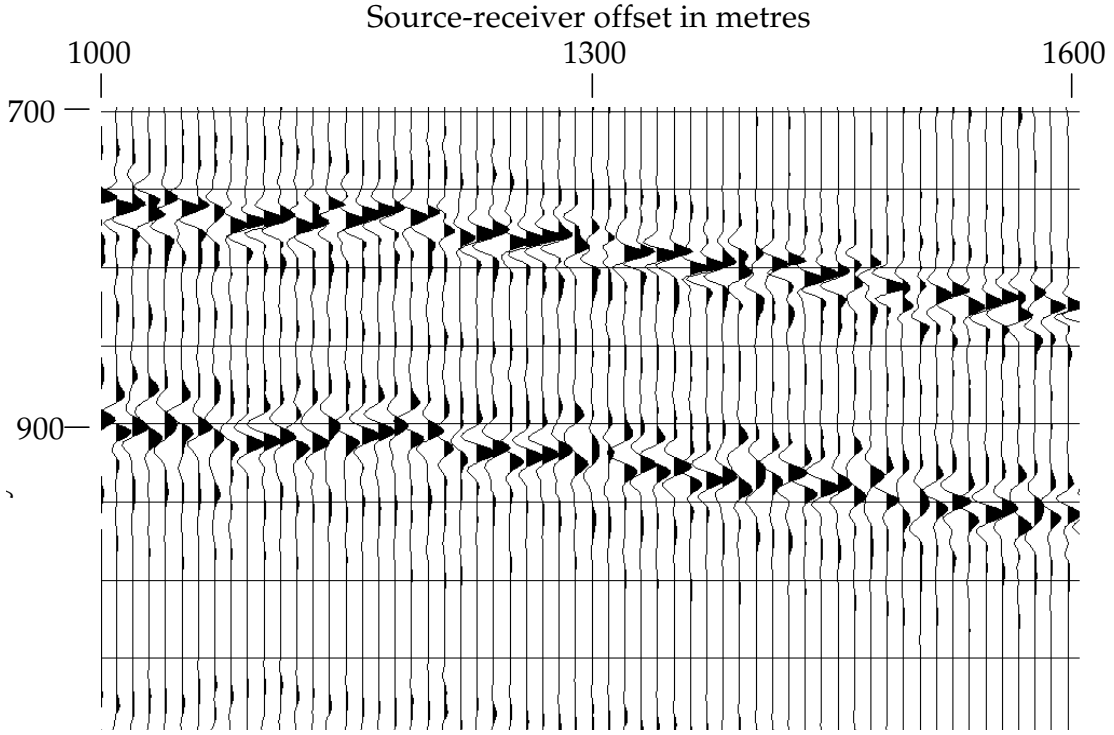

Figure 42 – Detail of synthetic gather with statics from the high velocity region of the R-T domain after two passes of R-T fan filter. Static shifts mostly preserved; filter tails filling blank zones.

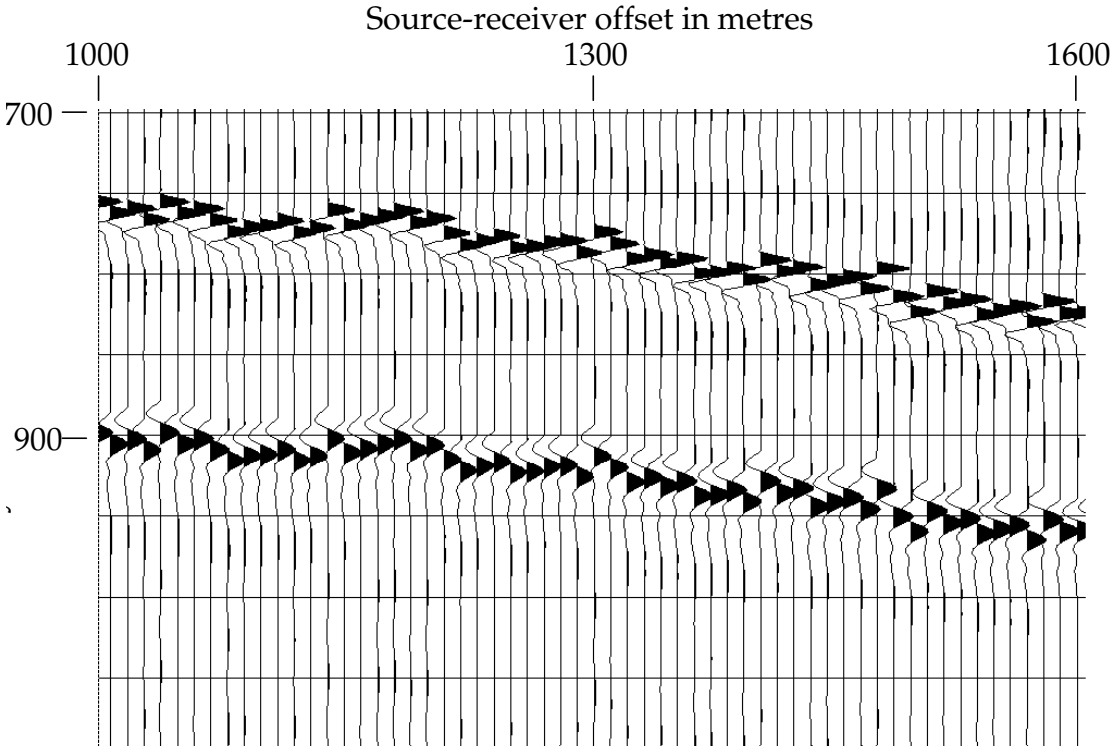

Figure 43 – Detail of synthetic gather with statics after application of F-K velocity reject filter. Statics and event amplitudes well preserved in this high velocity zone.

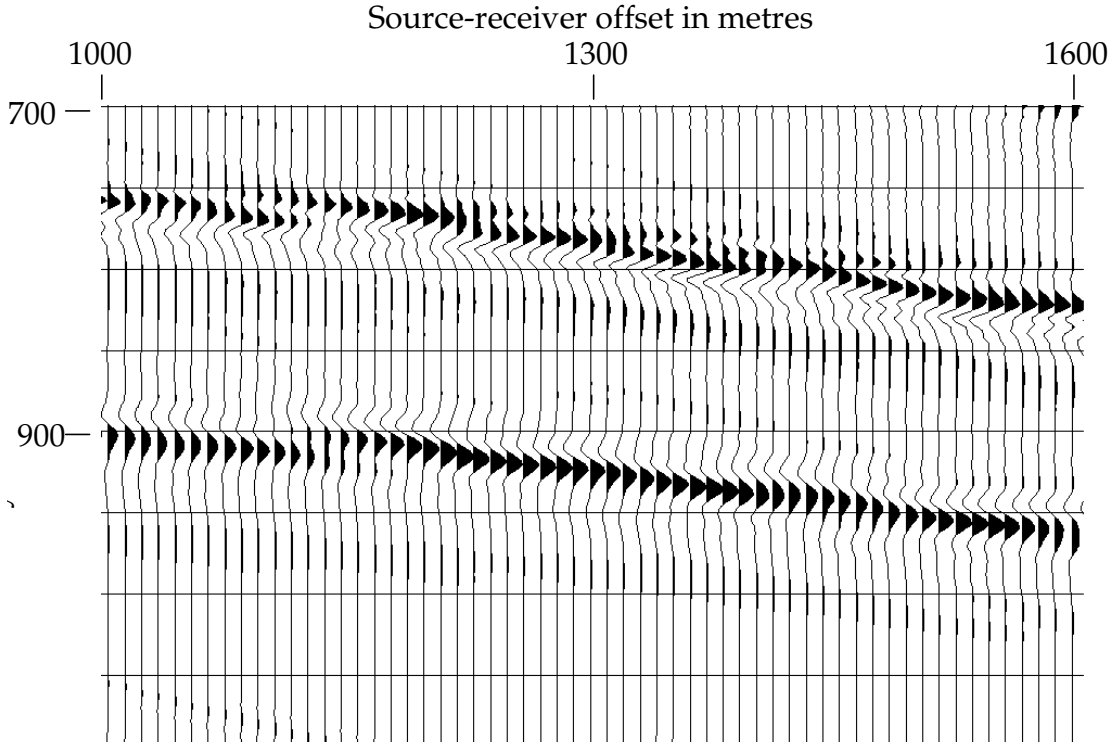

Figure 44 – Detail of synthetic gather with statics after application of F-K velocity boost filter. Static shifts totally smeared, and event amplitudes distorted.